Quaternary Science Reviews 219 (2019) 263–276

Contents lists available at ScienceDirect

Quaternary Science Reviews

journal homepage: www.elsevier.com/locate/quascirev

# $^{230}$Th/U burial dating of ostrich eggshell

Warren D. Sharp [a, *], Christian A. Tryon [b], Elizabeth M. Niespolo [a, c], Nick D. Fylstra [a], Alka Tripathy-Lang [a], J. Tyler Faith [d]

[a] Berkeley Geochronology Center, 2455 Ridge Road, Berkeley, CA 94709, USA
[b] Department of Anthropology, Harvard University, Cambridge, MA 02138, USA
[c] Department of Earth and Planetary Science, University of California, Berkeley, CA 94720, USA
[d] Natural History Museum of Utah and Department of Anthropology, University of Utah, Salt Lake City, UT 84108, USA

ARTICLE INFO

*Article history:*
Received 5 April 2019
Received in revised form
28 June 2019
Accepted 28 June 2019

*Keywords:*
Pleistocene
Geochronology
U-series
Archaeology
Africa
Middle stone age
Later stone age
Ostrich eggshells
Ratite eggshells

ABSTRACT

Obtaining precise and accurate dates for late Quaternary terrestrial sequences containing Middle Stone Age or Middle Paleolithic archaeological materials (ca. 30–300 ka) can be challenging. Many such sequences lie beyond the limit of radiocarbon dating (~50 ka) and lack volcanic ashes suitable for $^{40}$Ar/$^{39}$Ar dating. We report a dating approach with about ten times the range of radiocarbon dating (~500 ka) based on a novel protocol for $^{230}$Th/U dating of ostrich eggshell, a common component of African, Near Eastern and Asian archaeological sequences. Uranium in ostrich eggshell, typically at levels of tens to hundreds of ppb, is acquired after burial. However, accurate burial ages can be determined from measured $^{230}$Th/U ages when corrected for uranium uptake via diffusion. Using ostrich eggshells from a Pleistocene-Holocene east African site, we have: (1) characterized the spatial distribution of uranium and common thorium ($^{232}$Th) concentrations in ostrich eggshell by laser ablation ICP-MS, (2) determined apparent $^{230}$Th/U ages on outer and inner layers of eggshells by solution ICP-MS analyses of selectively abraded eggshells, and (3) calculated $^{230}$Th/U burial ages using a simple model for diffusive uptake of uranium. We assess our method by comparing the $^{230}$Th/U burial ages (median uncertainty 2.3%, 1 SD) with radiocarbon dates on carbonate from the same eggshells. We find good agreement in seven out of nine eggshells, confirming the accuracy of their $^{230}$Th/U model ages. Eggshells that fail to yield reliable $^{230}$Th/U ages may be recognized by anomalous patterns of apparent $^{230}$Th/U ages, providing a reliability criterion innate to the $^{230}$Th/U data. Ostrich eggshells are resistant to diagenesis simplifying $^{230}$Th/U dating compared to bones and teeth. Eggshells of ostrich, emu, rhea and other living and extinct ratites found on six continents share similar structure and composition, suggesting our new approach to $^{230}$Th/U dating of eggshell may be applicable in diverse late Quaternary terrestrial settings.

© 2019 Elsevier Ltd. All rights reserved.

## 1. Introduction

Studies of human behavioral and biological evolution and its paleoenvironmental context rely on accurate, precise dating of Quaternary terrestrial clastic sediments. For example, such dating is needed to: (1) assess the timing and tempo of cultural and biologic change recorded in stratified sequences, (2) correlate among stratigraphically discontinuous archaeological sequences, (3) evaluate relations among spatially separated paleoenvironmental, archaeological and fossil records, and (4) compare the timing of human development inferred from studies of ancient DNA with evidence from the archaeological or fossil records. Although many geochronometers are applicable to Quaternary terrestrial clastic sediments, as discussed below, dating at key archaeological sites remains challenging, especially at ages beyond the ca. 45–50 ka limit of radiocarbon ($^{14}$C) dating.

Eggshells of ratites (large, flightless birds including ostrich, emu and others) are common components of archaeological sequences in Africa, the Near East, Australia and elsewhere (e.g., Jain et al., 2016; McBrearty and Brooks, 2000; Miller et al., 1999; Miller et al., 2016; Rink et al., 2003; Wang et al., 2009). In Africa, ostrich eggshells brought back to human occupation sites may represent food debris, but these materials were also selected for use as often-decorated canteens (e.g., Diepkloof rockshelter, Texier et al., 2010)

* Corresponding author.
*E-mail addresses:* wsharp@bgc.org (W.D. Sharp), christiantryon@fas.harvard.edu (C.A. Tryon), eniespolo@berkeley.edu (E.M. Niespolo), nicholas.fylstra@ucalgary.ca (N.D. Fylstra), alka.trip@gmail.com (A. Tripathy-Lang), jfaith@nhmu.utah.edu (J.T. Faith).

https://doi.org/10.1016/j.quascirev.2019.06.037
0277-3791/© 2019 Elsevier Ltd. All rights reserved.

or as raw material for the production of disk-shaped beads used to adorn items and people.

Ratite eggshells can be highly suitable for $^{230}$Th/U dating (Magee et al., 2009). With favorable samples, $^{230}$Th/U dating is highly accurate and has a useful range of circa 500,000 years; i.e., ten times the range of $^{14}$C dating. The technique depends on simple mechanisms of radioactive decay, the relevant decay constants are precisely known (±0.3%, Cheng et al., 2013), and precise measurements (±1% or better) of $^{238}$U and its isotopic progeny $^{234}$U and $^{230}$Th are readily made on small samples (~0.1 g or less) using modern mass spectrometers. In contrast with luminescence techniques and electron spin resonance dating that require environmental dosimetry, $^{230}$Th/U dating requires measurements only of the sample itself, making it readily applicable to archival materials such as museum collections from prior excavations.

$^{230}$Th/U dating of ostrich and emu eggshells has been carried out for over 20 years (e.g., Magee et al., 1995; Miller et al., 1999; Rink et al., 2003; Roberts et al., 1994; Schwarcz and Morawska, 1993), however, previous studies have not taken into account that most uranium in buried eggshell is secondary. As a result, the reliability of $^{230}$Th/U ages on ratite eggshell has been uncertain. For example, if U uptake is prolonged, conventional $^{230}$Th/U ages on eggshell will be too young. If eggshells lose U after some has decayed to $^{230}$Th, their $^{230}$Th/U ages will be too old.

In this paper, we describe a novel approach that explicitly recognizes the secondary nature of U in buried eggshells, provides a means of correcting for prolonged U uptake, and aids in distinguishing between reliable and unreliable $^{230}$Th/U eggshells ages. We test our approach by comparing the resulting model ages, which we term "$^{230}$Th/U burial ages", with $^{14}$C ages on splits of the same eggshells (all <45 ka), showing that the $^{230}$Th/U ages are accurate.

### *1.1. Current limitations on dating late Quaternary terrestrial sequences*

Radiocarbon ($^{14}$C) dating, though enormously useful, is limited to the last ca. 50 ka, rendering most of African pre-history inaccessible to this technique. Moreover, despite AMS analyses and improved sample preparation protocols (e.g., Bronk Ramsey, 2008), the availability of specimens favorable for $^{14}$C dating is limited by factors such as poor preservation of bone collagen in tropical climates and degradation of charcoal due to storage in museum collections (Ambrose, 1998). Near the upper limit of its useful range of ca. 45–50 ka, $^{14}$C dating becomes extremely vulnerable to the effects of contamination by modern carbon, raising the possibility of obtaining misleading, finite $^{14}$C dates for samples that are actually much older (e.g., Miller et al., 2016).

The $^{40}$Ar/$^{39}$Ar dating technique is a bulwark of eastern African paleoanthropology but volcanic ashes of appropriate composition and mineralogy are commonly lacking at archaeological sites in southern and northern Africa, at many rockshelter sequences in Kenya and Tanzania —— e.g., Mumba (Gliganic et al., 2012) and Nasera (Ranhorn and Tryon, 2018) —— and in some open-air sequences in eastern Africa (e.g., Blegen et al., 2015). Recently, cryptotephra — volcanic material that is too fine or dilute to be detected by normal excavation techniques but can be correlated with dated ashes (Lane et al., 2015) —— has been recognized in African contexts. For example, glass shards from the ~74 ka Toba Tuff have been identified in cores from Lake Malawi (Lane et al., 2013) and at Pinnacle Point Cave in South Africa (Smith et al., 2018). Such finds provide highly precise tie points, however, the approach has been successfully applied at single levels in only a few African sites.

Luminescence techniques, including optically stimulated luminescence and thermoluminescence (OSL and TL) have undergone rapid development and widening application to archaeology in recent years as reviewed by Roberts et al. (2015). For example, luminescence dating has revolutionized our understanding of the timing and tempo of archaeological change at several MSA sites in South Africa and provided the age of the earliest reported remains of *H. sapiens* (Jacobs et al., 2008; Richter et al., 2017). Like all chronometers, luminescence techniques may be subject to systematic uncertainties arising from the depositional and lithological complexities of a given site. These include post-depositional mixing of grains across layers caused by plants, animals or hominids, the effects of beta microdosimetry in heterogeneous sediments, contamination by roof spall in rockshelters or caves, and other forms of inhomogeneous bleaching. Analyses of single grains of quartz accompanied by age modeling (e.g., Galbraith et al., 1999; Galbraith and Roberts, 2012; Jacobs et al., 2013) and/or dating of coexisting feldspar (e.g., Gliganic et al., 2012) can in many cases aid in resolving such effects. While widely applicable, luminescence techniques yield dates of relatively low external precision (generally, ± 5–10% at the 66% confidence level). As a result, luminescence dates may not be precise enough to closely assess relations between archaeological change and fluctuations in paleoclimate on timescales equal to or shorter than Earth's orbital precession cycles (~23 ka; e.g., Skonieczny et al., 2019). Luminescence dating, like other dosimetry techniques that require measurements of radiation fields in the vicinity of dating samples, are difficult or impossible to apply to archival materials.

ESR (electron spin resonance) dating (Grün, 2007) can be useful but precision is generally low (±10% or more at the 66% confidence level) and internal reliability criteria are not well developed. AAR (amino acid racemization) is also useful but is not a truly independent dating technique since ages from other geochronometers must be used to calibrate local temperature histories in order to apply AAR.

$^{230}$Th/U dating can provide precise and reliable ages for authigenic carbonates such as flowstones, stalagmites, buried soda straws, tufa, and calcrete (e.g., Hellstrom and Pickering, 2015; Marean et al., 2007; Sharp et al., 2016). However, suitable carbonates are absent from many archaeological sites, and relations between datable carbonate and archaeological materials may not be evident. Moreover, such ages commonly bracket, rather than directly date, human occupation of caves because conditions appropriate for abundant speleothem formation commonly alternate with those favoring human occupation (e.g., Pickering et al., 2019). $^{230}$Th/U dating of carbonate coatings on fossils and artifacts can provide a reliable minimum age for the coated object (e.g., Arsuaga et al., 2014; Hoffmann et al., 2018) if coatings are geochemically suitable (cf. Sharp and Paces, 2018) but such coatings are lacking in many archaeological contexts. $^{230}$Th/U dating of bones and teeth require consideration of secondary U mobility that is complicated by the highly reactive nature of bones and dentin in the burial environment (e.g., Grün et al., 2008; Kohn, 2008; Pike et al., 2002). Recent efforts to characterize U distribution in bones and teeth have benefited from rapid, spatially resolved analyses using laser ablation (e.g., Grün et al., 2014). However, convincing ages require substantial efforts for each sample (e.g., Holen et al., 2017).

We suggest that reliable $^{230}$Th/U dating of ostrich eggshells complements other chronometers presently in use. Below, we characterize the spatial distribution of U and common Th ($^{232}$Th) in modern and ancient ostrich eggshells, describe a protocol for $^{230}$Th/U dating of eggshell that explicitly accounts for secondary uranium, apply $^{230}$Th/U dating to Late Pleistocene-Holocene eggshells from an archaeological site in eastern Africa, and compare the resulting $^{230}$Th/U ages with $^{14}$C dates on carbonate from the same eggshells.

### 1.2. Site GvJm-22 at Lukenya Hill, Kenya

We have studied eggshells from a Middle to Later Stone Age archaeological sequence at site GvJm-22 in Kenya. The site is one of a number of rock shelters on an inselberg of Precambrian gneiss known as Lukenya Hill that rises ~100–200 m above the Athi-Kapiti Plain near Nairobi (see Fig. 1). The site was discovered and excavated in 1970–1973 by R. M. Gramly (Gramly, 1976) who recovered >50,000 stone artifacts and >3000 well-preserved faunal remains, including an *H. sapiens* partial calvaria (KNM-LH1). Materials from GvJm-22 are now archived at the National Museum of Kenya. As these are archival collections, recovery of *in situ* sediments for OSL dating was not possible and no cryptotephra were detected in analyses of sediment samples stored in Nairobi (McGuire, 2015). Materials from GvJm-22 have recently been studied further by Tryon et al. (2015), who described ostrich eggshell fragments, finished ostrich eggshell beads, and 'rough-outs' discarded during production. Those authors also provide a revised chronology for the GvJm-22 sequence based on 26 AMS $^{14}$C dates on the carbonate fraction of ostrich eggshell fragments. Splits from a subset of those eggshell fragments were analyzed in this study as described below under Methods. The eggshell fragments studied herein came from depths of 1.2–1.5 m below the present surface and are from the test pit of the excavation, which is located ~2 m from the shelter's rear wall and straddles the drip line (see Supplementary Information). See section 3.5 for $^{14}$C data from eggshells dated by $^{230}$Th/U in this paper. Additional information on site GvJm-22 is available in Tryon et al. (2015).

## 2. Methods

### 2.1. Laser ablation analyses

Spatial distributions of U and common Th ($^{232}$Th, half-life ~14 Ga) in ostrich eggshells were determined via laser ablation analyses using a Photon Machines Analyte II excimer laser and a Thermo-Fisher NEPTUNE *Plus* multi-collector inductively coupled plasma mass spectrometer.

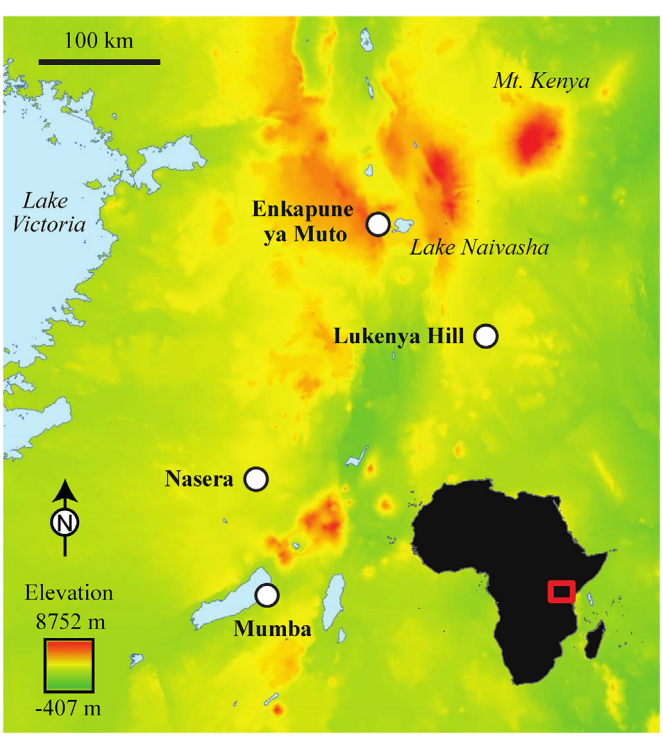


**Fig. 1.** Map of a region in eastern Africa showing location of Lukenya Hill, where site GvJm-22 is located, and other nearby rockshelters (white dots) with ostrich eggshells yielding ages near or beyond the $^{14}$C limit.

#### 2.1.1. $^{238}$U-$^{232}$Th profiles

U and common Th concentrations in all eggshells were determined along profiles perpendicular and parallel to their surfaces using eggshells that were cut, mounted in epoxy and polished. After pre-ablation to remove surface contamination with a 110 μm spot, 5% laser energy, 5 Hz repetition rate and 50 μm/s scan speed, the laser was operated in continuous scan mode using a 65 μm spot, 5 Hz repetition rate, 5 μm/s scan speed and 50% laser energy with 6.0 mJ (mJ) set point. $^{238}$U, $^{232}$Th and $^{43}$Ca were measured sequentially using magnetic field switching in cycles lasting ~7 s. U and Th were measured on an ion counter and the large $^{43}$Ca signal on a Faraday detector. We found that measuring the $^{238}$U/$^{43}$Ca ratio (rather than $^{238}$U intensity alone) provided more consistent results, presumably because using the ratio tends to correct for short term changes in ablation efficiency and instrumental sensitivity. U concentrations were determined by scaling the $^{238}$U/$^{43}$Ca ratios of eggshells to the $^{238}$U/$^{43}$Ca ratios obtained for a carbonate standard measured before and after each unknown; i.e. Grand Canyon travertine LC 190.3, a homogeneous carbonate containing ~2.5 ppm U (Mertz-Kraus et al., 2010).

#### 2.1.2. $^{238}$U-$^{232}$Th maps

$^{238}$U and $^{232}$Th concentrations in selected eggshells were mapped using closely spaced scans perpendicular to eggshell surfaces. Scans began and ended in epoxy to ensure coverage of the entire eggshell. After pre-ablation to remove surface contamination, the laser was operated in continuous scan mode, using a circular spot 110 μm in diameter, a 5 Hz repetition rate, 10 μm/s scan speed, and 100% laser energy with 6.0 mJ set point. The laser recorded precise x-y locations at 2-s increments during the main scan. $^{238}$U, $^{232}$Th and $^{43}$Ca were measured using the same method as above. Since peaks were measured sequentially, linear interpolation was used to associate $^{238}$U and $^{232}$Th intensities with $^{43}$Ca measurements. Before and after each eggshell analysis, gas blanks and Faraday baselines were measured and were subsequently averaged and subtracted from all measured intensities of each isotope. Backgrounds were generally less than 10 cps for $^{238}$U and $^{232}$Th and Faraday noise was $\leq$35 μV/s for $^{43}$Ca.

$^{43}$Ca intensity from each scan was used to determine when the laser spot completely intersected the eggshell, as indicated by a rapid rise and stabilization of signal intensity. A rapid decrease in signal intensity was used to identify the opposite edge of each eggshell. U concentrations were determined by scaling the $^{238}$U/$^{43}$Ca ratios of eggshells to the $^{238}$U/$^{43}$Ca ratios obtained for carbonate standard Grand Canyon travertine LC 190.3 measured before and after each unknown. Locations for each cycle are determined by comparing each cycle's time stamp to those collected every 2 s along each scan.

The result of this data reduction is a grid of concentrations that we use to generate a 2-D map. We process the data using an ordinary kriging algorithm with an exponential model in MATLAB. The data are interpolated at a mesh size of 1 μm × 1 μm and plotted as contoured color ramp plots. With this method of interpolation, a statistical model determines the spatial autocorrelation between measured points and provides the weights as a function of distance for the unknown locations (Matheron, 1973).

### 2.2. $^{230}$Th/U dating via ICP-MS analyses of solutions

Thin (~0.5 mm), tablet-shaped samples of eggshell located at

**Table 1**
$^{230}$Th/U analytical data and ages for ostrich eggshells from site Gvjm-22.

| Sample Name | Sample Wt. (mg) | U (ppb) | $^{232}$Th (ppb) | ($^{230}$Th/$^{232}$Th)[a] | ($^{232}$Th/$^{238}$U) | ± (%)[b] | ($^{230}$Th/$^{238}$U) | ± (%) | ($^{234}$U/$^{238}$U) | ± (%) | Uncorrected Age (ka)[c] | | Detritus-corrected Age (ka)[d] | | Initial ($^{234}$U/$^{238}$U)[e] | | Corrected Age (ka BP)[f] | |
|---|---|---|---|---|---|---|---|---|---|---|---|---|---|---|---|---|---|---|
| 120–130-A outer | 56.01 | 61.91 | 0.455 | 27.67 | 0.00144 | 0.16 | 0.0663 | 3.64 | 1.2671 | 0.71 | 5.85 | ±0.22 | 5.75 | ±0.23 | 1.272 | ±0.009 | 5.69 | ±0.23 |
| 120–130-A inner | 68.88 | 31.81 | 0.839 | 10.178 | 0.00663 | 0.07 | 0.0873 | 5.48 | 1.2794 | 0.32 | 7.69 | ±0.44 | 7.23 | ±0.50 | 1.287 | ±0.004 | 7.16 | ±0.50 |
| 130–140-A outer | 55.27 | 17.27 | 0.670 | 18.18 | 0.00864 | 0.20 | 0.2290 | 4.41 | 1.2100 | 0.66 | 22.74 | ±1.12 | 22.10 | ±1.17 | 1.225 | ±0.009 | 22.0 | ±1.2 |
| 130–140-A inner | 100.65 | 12.63 | 1.407 | 8.206 | 0.03228 | 0.09 | 0.2966 | 3.57 | 1.2320 | 1.20 | 29.77 | ±1.28 | 27.42 | ±1.76 | 1.258 | ±0.017 | 27.4 | ±1.8 |
| 130–140-B outer | 63.71 | 22.84 | 1.131 | 15.20 | 0.01303 | 0.06 | 0.2446 | 2.03 | 1.2106 | 0.42 | 24.46 | ±0.57 | 23.49 | ±0.75 | 1.227 | ±0.006 | 23.43 | ±0.75 |
| 130–140-B inner | 80.57 | 16.68 | 2.366 | 5.735 | 0.04224 | 0.15 | 0.2638 | 1.96 | 1.2252 | 0.82 | 26.25 | ±0.63 | 23.14 | ±1.73 | 1.249 | ±0.012 | 23.1 | ±1.7 |
| 130–140-C outer | 143.13 | 21.34 | 1.224 | 11.60 | 0.01698 | 0.18 | 0.2162 | 1.22 | 1.1840 | 0.83 | 21.87 | ±0.36 | 20.58 | ±0.75 | 1.198 | ±0.011 | 20.52 | ±0.75 |
| 130–140-C inner | 167.2 | 18.70 | 1.655 | 7.038 | 0.02624 | 0.11 | 0.1960 | 1.60 | 1.1505 | 1.30 | 20.29 | ±0.46 | 18.23 | ±1.15 | 1.162 | ±0.016 | 18.2 | ±1.2 |
| 130–140-D outer | 49.84 | 36.35 | 1.918 | 13.48 | 0.01451 | 0.22 | 0.2304 | 1.26 | 1.1870 | 1.14 | 23.39 | ±0.45 | 22.30 | ±0.71 | 1.202 | ±0.015 | 22.24 | ±0.71 |
| 130–140-D inner | 75.92 | 26.89 | 3.552 | 5.611 | 0.04025 | 0.12 | 0.2400 | 1.50 | 1.1883 | 0.46 | 24.46 | ±0.43 | 21.40 | ±1.65 | 1.207 | ±0.008 | 21.3 | ±1.6 |
| 140–150-A outer | 125.08 | 33.25 | 0.250 | 183.7 | 0.00159 | 0.54 | 0.4498 | 0.91 | 1.2208 | 0.33 | 49.36 | ±0.60 | 49.24 | ±0.60 | 1.254 | ±0.005 | 49.18 | ±0.60 |
| 140–150-A inner | 122.94 | 30.92 | 0.206 | 203.2 | 0.00126 | 0.11 | 0.4271 | 1.10 | 1.2027 | 0.96 | 47.19 | ±0.87 | 47.10 | ±0.87 | 1.232 | ±0.013 | 47.03 | ±0.87 |
| 140–150-B outer | 101.75 | 43.04 | 1.272 | 22.57 | 0.00847 | 0.09 | 0.2162 | 0.93 | 1.1969 | 0.31 | 21.60 | ±0.23 | 20.97 | ±0.40 | 1.210 | ±0.004 | 20.91 | ±0.40 |
| 140–150-B inner | 127.63 | 38.96 | 1.766 | 14.69 | 0.01366 | 0.06 | 0.2158 | 0.92 | 1.1938 | 0.34 | 21.63 | ±0.23 | 20.60 | ±0.58 | 1.208 | ±0.005 | 20.54 | ±0.58 |
| 140–150-C outer | 34.48 | 165.88 | 1.021 | 146.17 | 0.00135 | 0.23 | 0.2916 | 0.68 | 1.1743 | 0.45 | 30.89 | ±0.29 | 30.79 | ±0.30 | 1.190 | ±0.006 | 30.73 | ±0.30 |
| 140–150-C inner | 36.00 | 138.64 | 0.806 | 152.55 | 0.00119 | 0.22 | 0.2879 | 1.10 | 1.1685 | 0.25 | 30.63 | ±0.40 | 30.54 | ±0.40 | 1.184 | ±0.003 | 30.47 | ±0.40 |
| 140–150-D outer | 29.92 | 92.42 | 0.514 | 183.75 | 0.00086 | 0.16 | 0.3311 | 0.77 | 1.1926 | 0.28 | 35.14 | ±0.34 | 35.07 | ±0.34 | 1.213 | ±0.004 | 35.01 | ±0.34 |
| 140–150-D inner | 30.15 | 72.28 | 0.691 | 101.89 | 0.00171 | 0.40 | 0.3159 | 1.18 | 1.2009 | 0.31 | 33.00 | ±0.47 | 32.87 | ±0.47 | 1.221 | ±0.004 | 32.81 | ±0.47 |

[a] All isotope ratios are activity ratios. Decay constants are those of Jaffey et al. (1971) for $^{238}$U and Cheng et al. (2013) for $^{230}$Th and $^{234}$U.
[b] Uncertainties are given at two standard deviations.
[c] Uncorrected ages are calculated from measured ratios.
[d] Detritus-corrected ages were corrected for initial $^{230}$Th, $^{234}$U, and $^{238}$U using ($^{232}$Th/$^{238}$U) = 1.21 ± 0.50, ($^{230}$Th/$^{238}$U) = 1.0 ± 0.1, and ($^{234}$U/$^{238}$U) = 1.0 ± 0.1.
[e] Initial ($^{234}$U/$^{238}$U) is back-calculated from the measured ratio and the detritus-corrected $^{230}$Th age.
[f] Corrected age (ka BP) stands for kiloyears before present, where present is defined as 1950 A.D.

known distances from the eggshell surface were prepared by abrading with diamond and tool-steel dental burrs while using a micrometer to measure thicknesses. After abrasion, samples were coarsely crushed and pieces containing visible detritus, mostly from through-going pores, were removed using tweezers under a binocular microscope. The cleaned eggshell was then totally dissolved in 7N $HNO_3$ and equilibrated with a mixed spike containing $^{229}$Th, $^{233}$U, and $^{236}$U. The spike was calibrated using New Brunswick National Lab CRM145 uranium solution and solutions prepared from a 69 Ma U ore from Schwartzwalder Mine, Colorado, USA that has been demonstrated to yield concordant U-Pb ages (Ludwig et al., 1985) and sample-to-sample agreement of $^{234}$U/$^{238}$U and $^{230}$Th/$^{238}$U ratios. U and Th were separated from sample matrix using two stages of $HNO_3$–HCl cation exchange chemistry followed by reaction with $HNO_3$ and $HClO_4$ to remove any residual organic material. Procedural backgrounds for U and Th were measured with each batch of samples. U and $^{232}$Th from procedural backgrounds were negligible relative to sample U and $^{232}$Th. $^{230}$Th blanks, which averaged 0.00028 fmol, were subtracted from the measured $^{230}$Th.

Analyses were performed using a Thermo-Fisher NEPTUNE *Plus* multi-collector inductively coupled plasma mass spectrometer and CETAC Aridus II desolvator. U and Th fractions were analyzed simultaneously. Analyses were carried out in automated sequences, with each analysis consisting of a pre-analysis washout, an instrumental background measurement, a sample measurement, and a measurement of peak-tails. All measurements are normalized to simultaneous measurements of $^{238}$U to help cancel intensity fluctuations. Instrumental backgrounds at each U and Th mass, along with Faraday collector baselines and ion counter dark noise, were measured while aspirating the same dilute $HNO_3$-HF solution used to introduce samples. Sample measurements were carried out in peak-jumping mode with all masses measured on Faraday collectors except $^{230}$Th and $^{234}$U, which were measured with an ion counter. Sample measurements incorporated within-run mass bias corrections using the known $^{233}$U/$^{236}$U ratio of the spike. Faraday amplifier gains were calibrated weekly using the Neptune's constant current source and switching system. Ion counter yield (relative to Faraday collectors) were determined during each sample measurement by cycling $^{229}$Th and $^{233}$U between the ion counter and the L1 Faraday collector. Peak tails were monitored at seven half-mass positions from m/e = 229.5 to 241.5 while aspirating sample solution, and the sum of tails from all peaks was modeled at each U and Th mass position. Measured peak heights were corrected for Faraday baselines/ion counter dark noise, instrumental backgrounds, Faraday gains, ion counter yields, mass fractionation, peak-tails, procedural blanks, and interfering spike isotopes. The external reproducibility of $^{234}$U/$^{238}$U and $^{230}$Th/$^{238}$U ratios of Schwartzwalder Mine solutions measured during analytical sessions was better than 0.2% (2σ).

Activity ratios and ages were calculated using the half-lives of Jaffey et al. (1971) for $^{238}$U, Holden (1989) for $^{232}$Th, and Cheng et al. (2013) for $^{230}$Th and $^{234}$U. Correction for U and Th from detritus was made assuming detritus with activity ratios of ($^{232}$Th/$^{238}$U) = 1.2 ± 0.6 and ($^{230}$Th/$^{238}$U) = ($^{234}$U/$^{238}$U) = 1.0 ± 0.1 (Ludwig and Paces, 2002). Ages and uncertainties were calculated with Isoplot 3.75 (Ludwig, 2010). Uncertainties of corrected ages are reported at the 2σ-level and include measurement error, procedural $^{230}$Th blanks, and uncertainties associated with detritus corrections but not decay constants. Data and ages are reported in Table 1.

## 3. Results

### 3.1. Overview

Using laser ablation ICP-MS techniques, we have characterized the distribution of U in a modern ostrich eggshell obtained from an ostrich farm in southern California and in nine Late Pleistocene-Holocene ostrich eggshells from Middle to Later Stone Age archaeological deposits. The archaeological eggshells from site GvJm-22 at Lukenya Hill (Kenya) have significantly higher U concentrations than the modern shell and reveal distinctive patterns of $^{238}$U and $^{232}$Th (i.e., the relatively abundant primordial isotope of Th with half-life ~14 Ga) concentrations along profiles across the ~2-mm-thick shells.

Using solution ICP-MS techniques, we have determined $^{230}$Th/U ages of sub-samples from two positions in each of the archaeological eggshells. The sub-samples, which were prepared by selective abrasion, show systematic differences in $^{230}$Th/U ages across the thickness of the eggshells.

Using a simple model for diffusive uptake of U (Kohn, 2008), we show that the measured ages of most eggshells can be used to estimate the time when U uptake was initiated. We find that such "$^{230}$Th/U burial ages" are in good agreement with independently generated $^{14}$C dates on splits of the same eggshells.

### 3.2. Laser ablation profiling and mapping of $^{238}$U and $^{232}$Th in eggshells

We carried out laser ablation analyses of $^{238}$U and $^{232}$Th in eggshells in three configurations: (1) profiles normal to eggshell surfaces and internal layers, (2) traverses parallel to eggshell layers that cross relict eggshell pores, and (3) rectangular grids of closely-spaced analyses (scans) that were used to construct compositional maps of selected eggshells.

Laser ablation profiles normal to eggshell surfaces and internal layers (Fig. 2) reveal that modern eggshell contains ≤1 ppb U and that Holocene to Late Pleistocene archaeological eggshells from Lukenya Hill contain tens to hundreds of ppb of U. We interpret these relations to indicate that essentially all U in the archaeological eggshells is secondary. We infer that the archaeological eggshells, once buried, acquired secondary U by interaction with pore waters from surrounding sediments in a manner broadly similar to U uptake in buried bones and teeth (e.g., Kohn, 2008).

Examination of Fig. 2 shows that U concentrations vary systematically across the archaeological eggshells and define a strongly asymmetric pattern. Near the outer surfaces of eggshells, U concentrations are relatively high. Inward, U levels fluctuate or decrease smoothly for ~1100–1500 μm, plunge to the lowest levels observed in each shell, and then rebound near the inner surfaces of the shells. The pattern shows that U moves into eggshells from both outer and inner surfaces and suggests that uptake originating at the outer surface controls U concentrations across about three-fourths of the thickness of most shells; that is, from the outer surface to the position of the minimum U concentration observed in each shell.

In most shells, a marked transition in U concentration gradient occurs at about 1200–1500 μm from the outer surface. There, approximately constant or gently declining U concentrations in the outer shell give way to steeply dropping U values further inward. The rapid drop in U concentration coincides with a transition in the layered structure of ostrich eggshells; namely, the boundary between the palisade and mammillary cone layers (similar structures are present in most avian eggshells; e.g., Mikhailov, 1997). The palisade layer, which forms most of the outer part of the eggshell (see Fig. 3), consists of a comb-like array of elongated calcite crystals aligned parallel to each other and normal to the eggshell's outer surface. Individual low-Mg calcite crystals tens to hundreds of microns wide and ~1500 μm long extend across the entire palisade layer. In contrast, the mammillary cone layer consists of radiating clusters of prismatic or acicular calcite crystals originating from point sources of nucleation (mammillary knobs) at the inner surface of the mineral eggshell. During eggshell formation, the transition between the mammillary cone and palisade layers forms as most crystals radiating from adjacent centers of nucleation collide, leaving only those crystals oriented parallel to each other (and normal to the eggshell's outer surface) free to continue to grow. The strong parallel preferred orientation of calcite crystals in the palisade layer evidently favors transport of secondary U, perhaps due to enhanced fluid penetration along grain boundaries. We note that primary structures of the archaeological eggshells that we have studied and dated herein are readily visible in petrographic thin

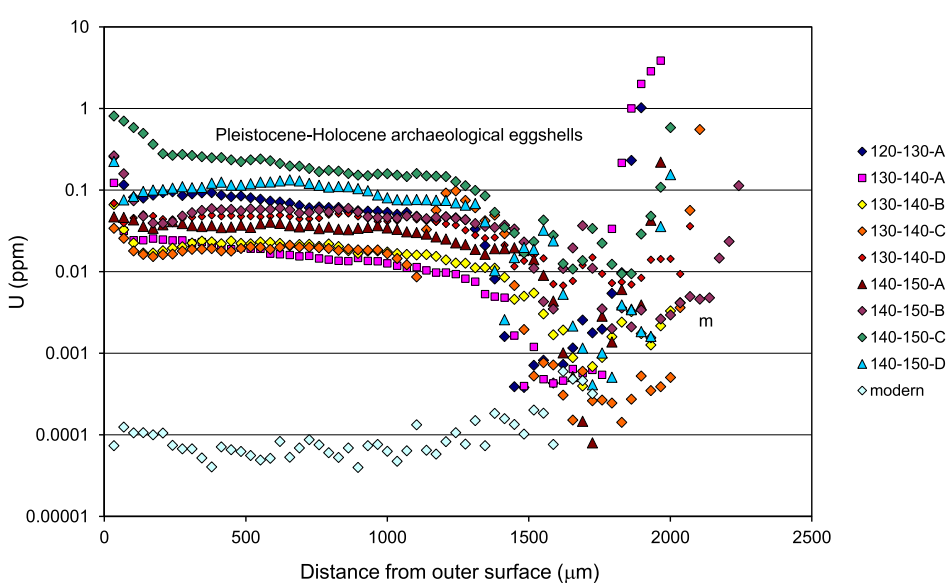


**Fig. 2.** U concentrations in ostrich eggshells versus distance from their outer surfaces; y-axis is logarithmic scale. Note low U in modern eggshell, higher U in Pleistocene-Holocene archaeological eggshells, and characteristic U concentration profiles across eggshells.

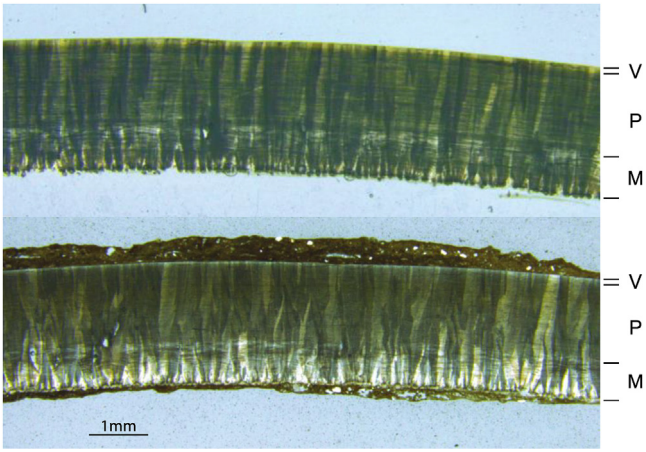


**Fig. 3.** Photomicrographs of thin sections of (upper) modern eggshell and (lower) archaeological eggshell 140-150-D ($^{14}$C age = 39.0–36.1 ka cal BP) with adhering detritus-rich soil carbonate. Labels indicate: V = vertical crystal layer; P = palisade layer; M = mammillary cone layer.

sections, indicating that such structure is preserved in eggshells tens of thousands of years old (see Fig. 3).

Most eggshells also have relatively steep U concentration gradients in the first 200–300 μm inward from the outer surface, giving way to flatter gradients further inward. Ostrich eggshells have a fine-grained layer at their outer surface, termed the vertical crystal layer, which is generally ~50 μm thick and consists of small (ca. 1–5 μm), randomly oriented equant crystals. In electron backscatter diffraction images of ostrich eggshell, such small, randomly oriented crystals gradually increase in proportion to the large crystals of the palisade layer in the outer ~300 μm of the ostrich eggshell, coincident with rapid increases in Mg that probably result from processes that lead to termination of formation of eggshell carbonate (Dalbeck and Cusack, 2006).

The steeper U gradients in the outer few hundred microns of eggshells suggest that the vertical crystal layer and the outermost palisade layer are associated with less rapid U transport than the remainder of the palisade layer. We speculate that the smaller, more equant, randomly-oriented crystals in the outer ~300 μm of the eggshell reduce the continuity of through-going fluid flow paths relative to those in the palisade layer, thereby inhibiting fluid (and U) uptake.

The laser ablation profiling of U shows that: 1) the transport of secondary U into eggshells is controlled in part by their layered structure, and 2) the relatively high and smoothly varying U concentrations found in carbonate from the palisade layer makes it especially suitable for $^{230}$Th/U dating.

$^{232}$Th/U ratios, which vary significantly across most eggshells, must also be considered in order to determine the suitability of eggshell carbonate for $^{230}$Th/U dating. $^{232}$Th/U ratios form U-shaped patterns with elevated values near the outer and inner surfaces of the archaeological eggshells (see Fig. 4). Elevated levels of $^{232}$Th near the surfaces of eggshells are associated with visible, fine-grained detritus that fills voids in eggshell carbonate. Such detritus contains extraneous $^{230}$Th; that is, $^{230}$Th not produced by decay of $^{238}$U in eggshell carbonate that must be subtracted in order to accurately calculate a $^{230}$Th/U age. While several protocols are available for doing so, for example, by using $^{232}$Th as an index and estimating the $^{230}$Th/$^{232}$Th or $^{238}$U/$^{232}$Th ratios of the detritus (e.g., Edwards et al. (2003); Ludwig and Paces (2002); see Methods for further details), uncertainties associated with these corrections tend to degrade the precision and accuracy of $^{230}$Th/U ages, especially if extraneous $^{230}$Th is a large fraction of the total $^{230}$Th present. Accordingly, eggshell carbonate with *low* $^{232}$Th/U ratios is most suitable for $^{230}$Th/U dating. For eggshells older than mid-Holocene, eggshell carbonate with $^{232}$Th/U ratios of $\leq 10^{-2}$, as found in carbonate from the palisade layers of most eggshells, is optimal for $^{230}$Th/U dating. Considering the observed patterns of U concentration (Fig. 2) and $^{232}$Th/U ratios versus distance from the surface in the archaeological eggshells (Fig. 4), we find that eggshell carbonate most suitable for $^{230}$Th/U dating occurs in the palisade layer at distances from the outer surface of circa 500–1300 μm with some variation in the optimal position from shell to shell.

Macroscopic pores that provide paths for gas exchange during development of ostrich embryos are present in modern and archaeological eggshells (see Fig. 5). They form roughly circular openings a few mm in diameter on the outer shell surface and extend partly or completely through the eggshell carbonate, usually at high angles to its layered structure (Mikhailov, 1997). In the archaeological eggshells from Lukenya Hill, such pores are partially or completely filled by secondary carbonate and detritus. Detritus in relict pores, if not removed, will degrade the suitability of eggshell carbonate for $^{230}$Th/U dating, and secondary carbonate in relict pores may have formed diachronously relative to U uptake in surrounding eggshell carbonate, complicating interpretation of $^{230}$Th/U dates (e.g., Loewy et al., 2017; Niespolo et al., 2017a). Furthermore, pores may provide enhanced access to eggshells by soil water, affecting U transport into the adjacent eggshell carbonate. Accordingly, to assess the effects of pores and relict pore fillings on the U-Th systems of Lukenya Hill eggshells, we measured U and $^{232}$Th/U ratios in selected samples along laser ablation traverses *parallel* to eggshell surfaces (Fig. 5). These measurements also help to evaluate the uniformity of U concentrations at constant distances from the outer surface. Our results show that U concentrations and $^{232}$Th/U ratios remain nearly constant along each traverse except where punctuated by higher U and $^{232}$Th/U ratios associated with secondary carbonate and detritus that fill relict eggshell pores. The elevated U and $^{232}$Th/U ratios of the detritus and secondary carbonate filling relict pores confirms that these materials should be removed prior to analysis so they do not degrade primary eggshell carbonate for $^{230}$Th/U dating. The higher U concentrations associated with relict pores are of limited extent, however. They extend only about 0.5 mm from the center of the pores, indicating that the pores did not act as major conduits for U enrichment of the surrounding primary eggshell carbonate. We infer that secondary carbonate in relict pores may have formed rapidly upon burial, sealing the pores from further fluid flow.

In subsequent work, we have adopted the practice of removing visible pore fillings by selective abrasion and/or drilling followed by hand cleaning of the abraded and crushed carbonate via inspection under a low power microscope.

The laser traverses parallel to eggshell layers also confirm that U concentrations and $^{232}$Th/U ratios are relatively uniform in the layer-parallel direction (aside from the pores); that is, U decreases uniformly with distance away from the eggshell's outer surface in the eggshells shown in Fig. 5.

Fig. 6 shows laser ablation maps of U concentration and $^{232}$Th/U ratios for regions of two eggshells 140–150-C (Fig. 6A) and 130–140-A (Fig. 6B). Fig. 6A shows that patterns of U concentration and $^{232}$Th/U ratio in this shell are relatively continuous parallel to the surface of the shell, while Fig. 6B shows a more complex distribution. For example, U concentrations near the outer surface of 130–140-A (Fig. 6B) are highly variable and other loci of high U within the palisade layer form discontinuous “hotspots” unrelated to the layered structure of the eggshell or its visible pores. We interpret these features to indicate that 130–140-A (Fig. 6B) had a more complex history of U mobility than 140–150-C (Fig. 6A). As

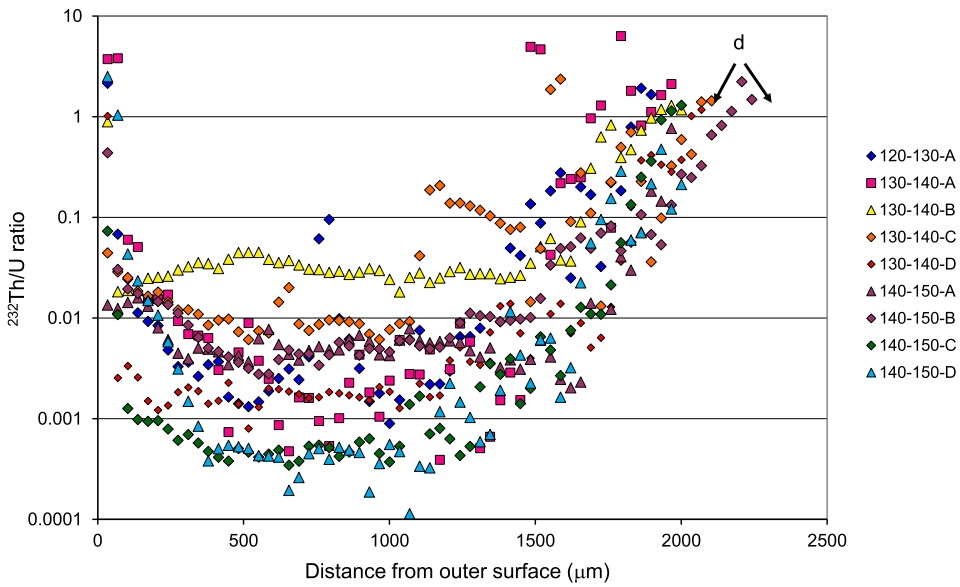


**Fig. 4.** $^{232}$Th/U ratios of ostrich eggshells versus distance from their outer surfaces. Note high $^{232}$Th/U ratios adjacent to eggshell surfaces and $^{232}$Th/U ratios <0.01 in their interiors, making the latter favorable for $^{230}$Th/U dating.

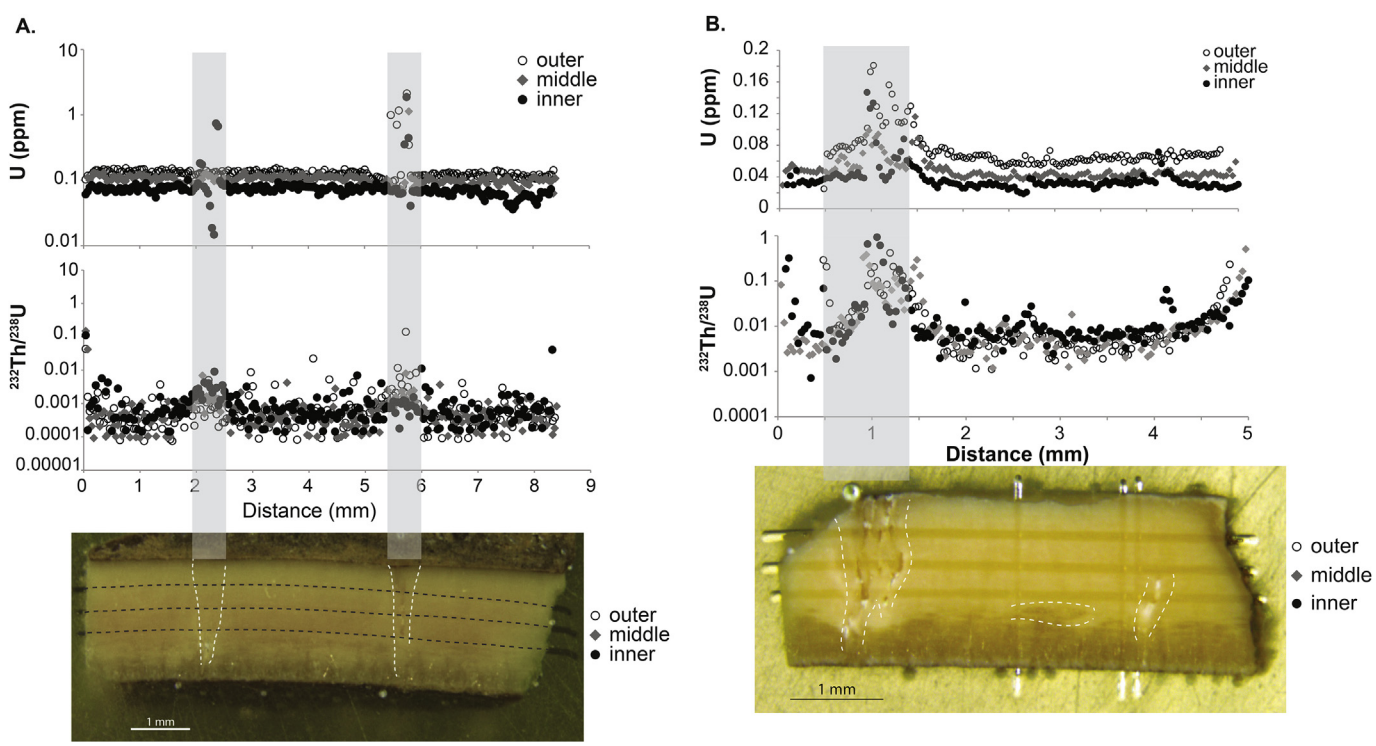


**Fig. 5.** U concentrations and $^{232}$Th/U ratios measured along laser ablation traverses parallel to eggshell layers. A.(bottom panel) Photo shows archaeological eggshell 140-150-D cut normal to internal layers, mounted in epoxy, and polished for laser ablation analysis. Dashed black lines show traverses along the outer, middle, and inner palisade layer of the eggshell. Dashed white lines highlight relict eggshell pores. A.(upper and middle panels) U concentrations and $^{232}$Th/U ratios, respectively, measured along the three traverses. Except across pores, U is relatively uniform along each traverse and decreases progressively with distance from the outer surface. High or erratic U concentrations and high $^{232}$Th/U ratios coincide with relict pores at positions highlighted by vertical gray bands. **B.**(bottom panel) Photo of archaeological eggshell 120–130-A, prepared as above. Laser traverses are visible as horizontal lines in photo and dashed white lines highlight relict eggshell pores. B.(upper and middle panels) U concentrations and $^{232}$Th/U ratios, respectively, measured along the outer, middle and inner palisade layer. U is relatively uniform along each traverse and decreases progressively with distance from the outer surface except in the vicinity of the large relict pore near 1 mm. High U concentrations and high $^{232}$Th/U ratios coincide with the relict pore as highlighted by the vertical gray band. $^{232}$Th/U ratios also increase near the right edge of the eggshell fragment that was exposed to soil during burial.

discussed in section 3.3 below, the different distributions of U in these two eggshells are associated with distinct apparent $^{230}$Th/U age distributions and suitability for dating.

The map of $^{232}$Th/U ratios for 140–150-C (Fig. 6A, right panel) shows that the region of low $^{232}$Th/U ratios that is most favorable for $^{230}$Th/U dating lies within the central region of this eggshell

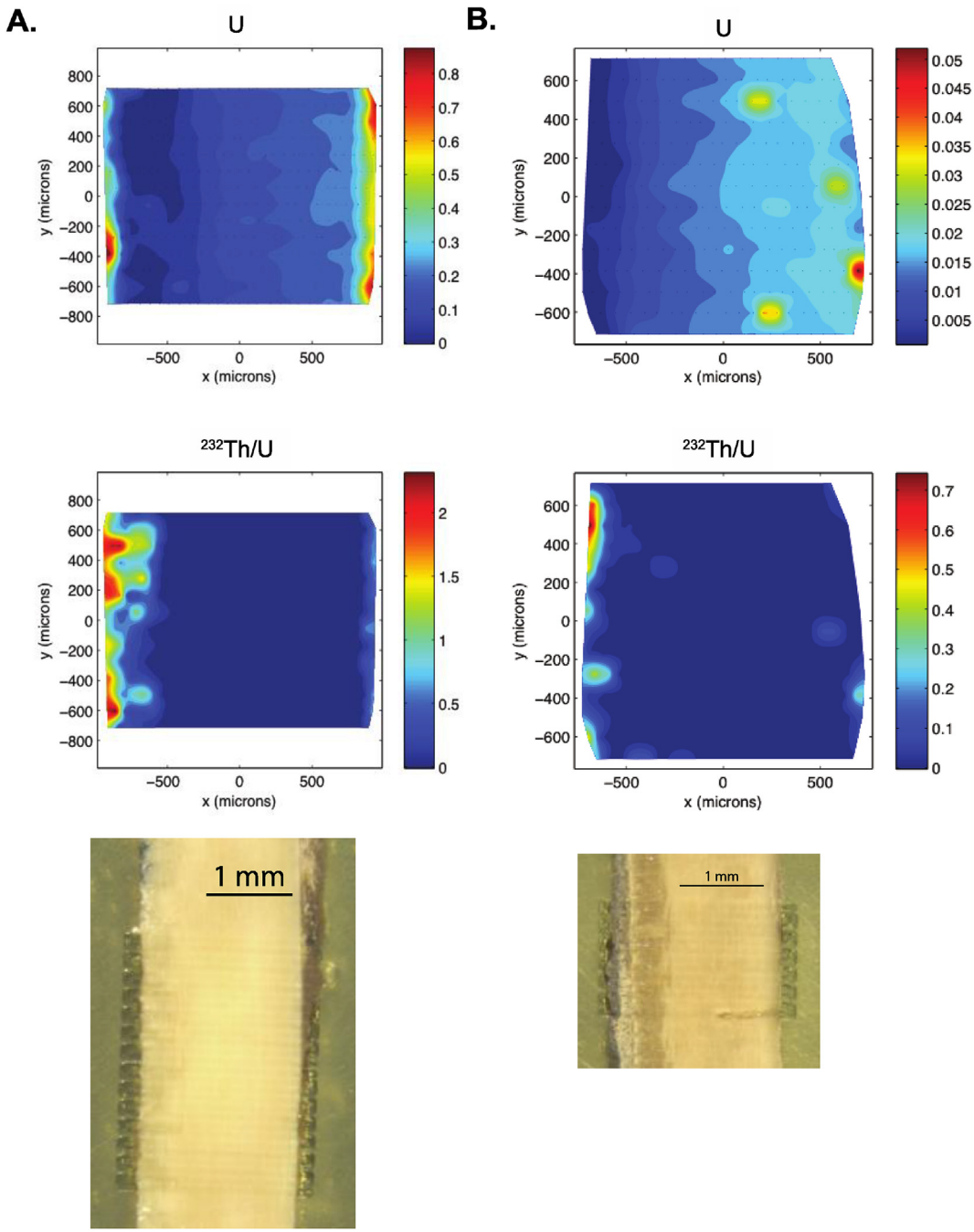


**Fig. 6.** Laser ablation maps of relative U concentrations and $^{232}$Th/U ratios for two archaeological eggshells with contrasting patterns of $^{230}$Th/U apparent ages (see text). Warm colors indicate higher values; outer surfaces of eggshells are on the right. (A) Maps of relative U concentration and $^{232}$Th/U ratios (upper and middle panels, respectively) and photo of analyzed area of eggshell 140–150-C (lower panel). Maximum U concentration in eggshell 140–150-C is ~0.95 ppm. (B) Maps of relative U concentration and $^{232}$Th/U ratios (upper and middle panels, respectively) and photo of analyzed area of eggshell 130–140-A (lower panel). Maximum U concentration in eggshell 130–140-A is ~0.11 ppm.

occupied by the palisade layer. That is, although the highest U concentrations occur in the first few tens of microns from the eggshell's outer surface, $^{232}$Th concentrations in that region are also high, leading to elevated $^{232}$Th/U ratios unfavorable for dating. Both eggshells show that carbonate near their inner surfaces can have high $^{232}$Th/U ratios making it desirable to exclude such material from $^{230}$Th/U dating samples.

### 3.3. $^{230}$Th/U dating

Carbonate from the palisade layers of eggshells from site GvJm has U concentrations of ~170 ppb or less (Table 1); hence, the minor isotopes of interest for $^{230}$Th/U dating (i.e., $^{234}$U and $^{230}$Th), which are present at levels $>10^4$ and $\sim10^5$ times *lower* that $^{238}$U, are too low for precise measurement via laser ablation. Accordingly, solution ICP-MS techniques were applied to ca. 30–150 mg samples prepared by selective abrasion of the eggshells. Two fractions of

carbonate were dated from each of nine archaeological eggshells. Carbonate visibly contaminated by detritus near the eggshell's outer surface and in the mammillary cone layer was first removed by abrading with stainless steel dental burrs. Then tablets of eggshell ~0.5 mm in thickness from two positions within the palisade layer of each eggshell were prepared by further abrasion while using a micrometer to monitor the thickness of the material removed. These carbonate fractions were centered, respectively, at positions about 30% and 70% across the palisade layer measured from the eggshell's outer surface. We term these "outer shell" and "inner shell" fractions, respectively, but emphasize that both fractions are derived from the palisade layer. The tablets were ultrasonically cleaned, gently crushed, further cleaned under a binocular microscope by removing any remaining pieces of eggshell that contained visible detritus, and then analyzed via ICP-MS. See Methods for details of chemistry, mass spectrometry, and data reduction.

Measured U concentrations in the archaeological eggshells range from ~13 to 166 ppb (median, 33 ppb), $^{232}$Th concentrations from ~0.21 to ~3.6 ppb (median, 1.1 ppb), and ($^{230}$Th/$^{232}$Th) activity ratios from 5.6 to >200 (median, ~17), indicating that the carbonate from most eggshells is compositionally suitable for U-Th dating (See Table 1). As expected from the laser ablation results, the U concentrations of outer shell fractions, which range from ~166 to 17 ppb (median, ~36 ppb), are consistently higher than those of corresponding inner shell fractions, which range from ~139 to 13 ppb (median, ~29 ppb).

Detritus-corrected $^{230}$Th/U ages range from $5.69 \pm 0.23$ to $49.18 \pm 0.60$ ka BP (i.e., relative to A.D. 1950) and have a median calculated error of ~3% while favorable samples have errors as small as ±1% (all errors are 2σ). Initial $^{234}$U/$^{238}$U activity ratios (back calculated from measured $^{234}$U/$^{238}$U ratios and ages) vary from ~1.16 to 1.29. Such $^{234}$U/$^{238}$U ratios, which are modestly enriched relative to secular equilibrium, are similar to those observed for some pedogenic carbonates, which also contain U derived from vadose zone pore waters (e.g., Ludwig and Paces, 2002; Oerter et al., 2016; Sharp et al., 2003).

The $^{230}$Th/U ages were determined on splits from the same eggshell fragments dated by Tryon et al. (2015) using $^{14}$C on eggshell carbonate. Radiocarbon dates for the carbonate fraction of eggshells of ostriches and other ratites determined on acid-etched samples via AMS are considered reliable (e.g., Bird et al. (2003); Janz et al., 2009; Magee et al. (2009); Vogel et al., 2001) and replicate analyses of eggshells from site GvJm-22 by two labs (University of Arizona and Queen's University Belfast) yielded indistinguishable results. See Table 2 for $^{14}$C ages of samples dated in this paper. The $^{14}$C ages therefore provide robust ages of formation for the archaeological eggshells with which our $^{230}$Th/U ages may be compared. By mutual agreement, the $^{230}$Th/U ages of the eggshells were determined without prior knowledge of their $^{14}$C ages. That is, $^{230}$Th/U dating of the eggshells constituted a "blind experiment".

$^{230}$Th/U ages (both measured ages and "burial ages", see discussion below) and $^{14}$C ages are plotted in Fig. 7. Most eggshells (except 120–130-A and 130–140-A, discussed further below) display a similar pattern of ages: $^{230}$Th/U ages of inner-shell fractions are ≤ $^{230}$Th/U ages of outer-shell fractions, which are ≤ $^{14}$C ages of eggshell carbonate. Such a pattern is expected if, upon burial and exposure to U-bearing soil water, U entered the palisade layer via the outer surface of the eggshell, became progressively enriched in the interior with time, and, once fixed at a given position, decayed in place to produce $^{230}$Th that remained where it formed by radioactive decay.

Two (of nine) eggshells have $^{230}$Th/U inner shell ages > $^{230}$Th/U outer shell ages, a relation inconsistent with a simple U uptake history such as the one outlined above. Furthermore, the $^{230}$Th/U ages of the inner shell of 120–130-A and both fractions of 130–140-A are older than their $^{14}$C dates. Such anomalously old $^{230}$Th/U ages could result if U uptake and ensuing decay to $^{230}$Th were followed by later loss of U. As discussed above, laser ablation mapping of 130–140-A (Fig. 6b) reveals a U distribution that is more complex than in 140–150-C, which yields ages and a spatial distribution of U consistent with single-stage U uptake. We suggest that the patchy U distribution in 130–140-A seen in Fig. 6 may reflect complex or multi-stage U transport that has rendered the eggshell unsuitable for accurate $^{230}$Th/U dating. Alternatively, the anomalously old $^{230}$Th/U ages could result from inadequate correction for initial $^{230}$Th; however, we consider this explanation less likely. (See Methods for a description of the $^{232}$Th-based model correction that was applied.)

Considering the seven eggshells with inner shell $^{230}$Th/U ages ≤ $^{230}$Th/U outer shell ages, inspection of Fig. 7 shows that in all cases the outer shell $^{230}$Th/U ages provide accurate minimum estimates of eggshell ages given by the $^{14}$C dates. The $^{230}$Th/U ages of some eggshells closely approach or equal their $^{14}$C ages while in other cases outer shell $^{230}$Th/U ages are distinctly younger than the associated $^{14}$C ages. For example, 130–140-B has outer shell $^{230}$Th/U and $^{14}$C ages, respectively, of $23.43 \pm 0.75$ ka and 24.00 to 23.36 ka cal BP (UBA-23929, Table 2), in good agreement. In contrast, 140-150-D has outer shell $^{230}$Th/U and $^{14}$C ages of $35.01 \pm 0.34$ ka and 39.00 to 36.10 (UBA-23935, Table 2), respectively, indicating that it is likely that the outer shell $^{230}$Th/U age underestimates the $^{14}$C age of the eggshell by ca. 2 ka or more (about 5%).

### 3.4. Determining $^{230}$Th/U burial ages

In order to determine if improved estimates of eggshell ages could be obtained from the $^{230}$Th/U data, we applied diffusion modeling to correct for the effect of prolonged U uptake. We assume that uptake of secondary U commences upon burial and ensuing exposure to U in sediment pore waters, hence we term the resulting model ages "$^{230}$Th/U burial ages".

The process of diffusion has been shown to provide a useful physiochemical and mathematical framework for modeling U uptake during diagenesis of biominerals such as bones and teeth (e.g., Kohn, 2008; Millard and Hedges, 1996; Pike et al., 2002; Sambridge et al., 2012). To our knowledge, U uptake in ratite eggshell has not previously been modeled. The mechanisms by which U is transported and fixed in eggshell are as yet unknown and may well be distinct from the processes responsible for U uptake in bones and teeth, given the differences in composition (Ca-phosphates in bones and teeth versus carbonate in eggshells), primary organic content (~20–40% in bone, ~20–33% in dentin, and ~4% in enamel versus ~3% in eggshell), and crystal shape and size (nm-scale platelets in bones and nm-to μm-scale rods in enamel versus equant or acicular crystals tens to hundreds of μm in size in ratite eggshell) (cf. Dalbeck and Cusack, 2006; Elliott, 2002; Mikhailov, 1997; Trueman and Tuross, 2002). We assess $^{230}$Th/U burial ages by comparing them with $^{14}$C dates on splits of the same eggshells, providing a robust test of our results.

The region of a biomineral near its surface will be first to equilibrate with incoming U while interior regions will equilibrate more slowly. It follows that dates measured near the surface of a biomineral will most closely approximate its true age, assuming a single stage of U uptake and no subsequent U loss (e.g., Pike et al., 2002, Fig. 2A in Kohn, 2008). In ostrich eggshells that have been buried, however, near-surface carbonate is generally unsuitable for $^{230}$Th/U dating because it is rich in detritus derived from the surrounding sediments, leading to large, model dependent corrections for initial $^{230}$Th. Accordingly, $^{230}$Th/U ages were measured in the

**Table 2**
$^{14}$C dates and $^{230}$Th/U burial ages of ostrich eggshells from site GvJm-22.

| Sample ID | Lab ID | $^{14}$C yr BP (±1s)[a] | $^{14}$C yr cal BP (95%)[b] | $^{14}$C ka cal BP (95%)[c] | $^{230}$Th/U Burial Ages (ka BP)[d] | (+, ka, 95%) | (-, ka, 95%) |
|---|---|---|---|---|---|---|---|
| 120–130-A | UBA-23927 | 4448 ± 32 | 5276–4872 | 5.28–4.87 | na | | |
| 130–140-A | UBA-23928 | 12884 ± 59 | 15,593–15,157 | 15.6–15.2 | na | | |
| 130–140-B | UBA-23929 | 19666 ± 120 | 23,996–23,355 | 24.0–23.4 | 23.9 | 2.7 | 1.2 |
| 130–140-C | UBA-23930 | 19594 ± 119 | 23,924–23,226 | 23.9–23.2 | 23.6 | 2.6 | 2.6 |
| 130-140-D | UBA-23931 | 19794 ± 127 | 24,118–23,488 | 24.1–23.5 | 23.4 | 2.7 | 1.8 |
| 140–150-B | UBA-23933 | 19568 ± 119 | 23,888–23,180 | 23.9–23.2 | 21.44 | 1.2 | 0.87 |
| 140–150-C[e] | UBA-23934 | 28041 ± 320 | 32,792–31,247 | 32.8–31.3 | 31.12 | 1.0 | 0.63 |
| | AA102890 | 28230 ± 380 | 33,174–31,304 | 33.2–31.3 | | | |
| 140-150-D[f] | UBA-23935 | 33308 ± 612 | 39,002–36,103 | 39.0–36.1 | 37.9 | 1.6 | 1.6 |
| | AA102889 | 33140 ± 570 | 38,721–36,042 | 38.7–36.0 | | | |
| 140–150-A[g] | UBA-23932 | 46710 ± 3852 | 50,000–45,201* | 50.0–45.2 | 52.0 | 2.1 | 2.1 |
| | | | 54,050–45,430 # | 54.1–45.4 | | | |

[a] $^{14}$C dates are from Tryon et al. (2015), are on the carbonate fraction of ostrich eggshells, and are reported as mean and 1 standard deviation. Laboratory codes: UBA, Queen's University Belfast; AA, University of Arizona.
[b] $^{14}$C dates were calibrated using OxCal v.4.3.2 (Bronk Ramsey, 2017) and a combined IntCal13/SH13Cal13 calibration curve after Tryon et al. (2018) and are reported at 95.4% uncertainty, in years before A.D. 1950.
[c] Calibrated $^{14}$C dates expressed in ka and rounded to 3 figures for ease of comparison with $^{230}$Th/U burial ages.
[d] See text for calculation of $^{230}$Th/U burial ages and errors; ages are reported relative to A.D. 1950.
[e] $^{14}$C analyses of this specimen were obtained from two labs, UBA and AA.
[f] $^{14}$C analyses of this specimen were obtained from two labs, UBA and AA.
[g] The uncalibrated $^{14}$C date UBA-23932: 46,710 ± 3852 BP straddles the upper limit of the IntCal13/SH13Cal13 calibration, yielding a calibrated date with an upper limit truncated at 50,000 yr cal BP, marked with (*). A calibrated date determined using atmospheric $^{14}$C/$^{12}$C data from Hulu Cave stalagmites (Cheng et al., 2018) is marked with (#).

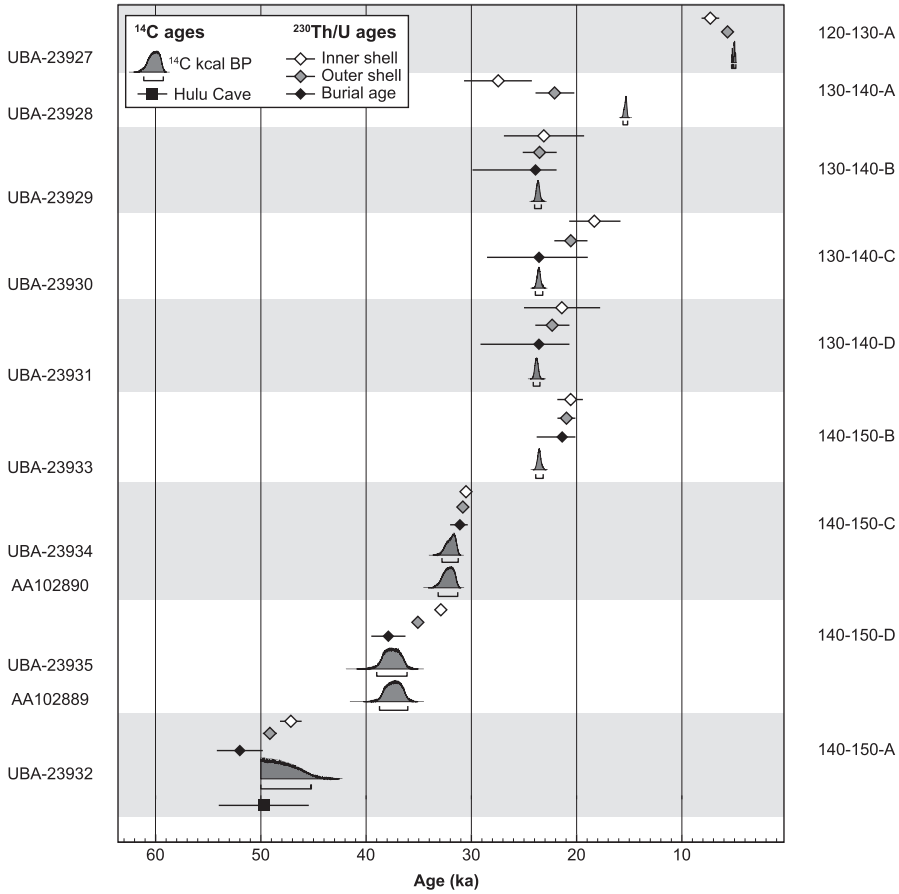


**Fig. 7.** $^{230}$Th/U ages of ostrich eggshells from site GvJm-22 compared with the calibrated $^{14}$C ages of carbonate fractions of the same eggshells; all ages are before present, where present is 1950. Measured $^{230}$Th/U ages of inner and outer shells are shown in open and gray diamonds, respectively. $^{230}$Th/U burial ages (see text section 3.4) are shown in black diamonds. $^{14}$C ages calibrated via IntCal13/SHCal13 are shown as probability density functions. An alternate calibration for sample 140–150-A, which straddles the upper age limit of the IntCal13/SHCal13 calibration, uses the data of (Cheng et al., 2018) from Hulu Cave and is shown as a black square. All errors are ±95%. $^{14}$C dates are from Tryon et al. (2015).

interior of the palisade layer where the eggshell is generally highly suitable for $^{230}$Th/U dating. Conceptually then, the problem is to extrapolate from ages measured at positions in the interior to the age expected at the surface of the eggshell. Kohn (2008) has shown that a variety of diffusion-limited mechanisms (e.g., diffusion-adsorption, diffusion plus reaction or recrystallization, and

double-medium diffusion) follow similar mathematical relations that, in this case, relate (1) the measured $^{230}$Th/U ages, (2) their positions, and (3) the model age at the eggshell's outer surface (i.e., the $^{230}$Th/U burial age). Kohn (2008) also has shown that if measured ages are regressed with respect to normalized distance squared (rather than distance), a linear relationship between measured ages and their positions is expected (see Fig. 2C in Kohn, 2008). Thus, the age of initial U uptake may be determined from the regression intercept and age-errors may be determined using straightforward linear regression diagnostics.

We determined $^{230}$Th/U burial ages for seven Lukenya Hill eggshells with $^{230}$Th/U ages that become younger inward; i.e., that are consistent with single-stage U uptake. To determine regression intercepts ($^{230}$Th/U burial ages), we regressed measured $^{230}$Th/U ages versus normalized distance across the palisade layer, where normalized distance = 1-X'$^2$, X' = X/L and L = edge-core distance (see Fig. 8). We took the outer eggshell surface as the edge and the minimum in U concentration near the boundary of the palisade and mammillary cone layers as the core (Fig. 2). Errors in both positions and measured ages of samples were propagated into the error in the regression intercept. We assume that outer shell $^{230}$Th/U ages provide a minimum age for the eggshells. Thus we have constrained errors on the young side of $^{230}$Th/U burial ages to coincide with errors of the corresponding outer shell $^{230}$Th/U ages. As a result, some $^{230}$Th/U burial ages have asymmetric errors. The resulting $^{230}$Th/U burial ages are plotted in Fig. 7.

### 3.5. Comparing $^{230}$Th/U burial and $^{14}$C dates

We find good agreement between $^{230}$Th/U burial dates and $^{14}$C ages in most eggshells (see Fig. 7, Table 2). Six eggshells have $^{230}$Th/U burial dates that agree with their $^{14}$C ages within stated uncertainties. The $^{230}$Th/U burial date of one eggshell (140–150-B) underestimates the corresponding $^{14}$C age by ~2 ka although when uncertainties are considered the underestimate is < 1 ka. We interpret these relations to indicate that a diffusion-limited model of U transport can be used to infer the timing of initial U uptake in eggshells, and that $^{230}$Th/U burial dates provide improved estimates for eggshell ages compared to measured $^{230}$Th/U ages.

It is useful to consider the relationship between $^{230}$Th/U burial dates and the archaeological event that we wish to date; i.e., in the present case, hominin use of the ostrich egg or eggshell. While time clearly must elapse between eggshell formation, burial and ensuing U uptake, that interval is evidently smaller than the uncertainties of our ages for the Lukenya Hill eggshells. That is, hominin utilization of the eggshells must have occurred between eggshell formation, dated by $^{14}$C ages of eggshell carbonate, and onset of U uptake in the burial environment, dated by the $^{230}$Th/U burial ages. Thus, the good agreement between $^{14}$C and $^{230}$Th/U burial ages observed for the Lukenya Hill eggshells indicates there is close coincidence between the "target event" (hominin eggshell usage) and the "dated event" (the $^{230}$Th/U burial ages of the eggshells).

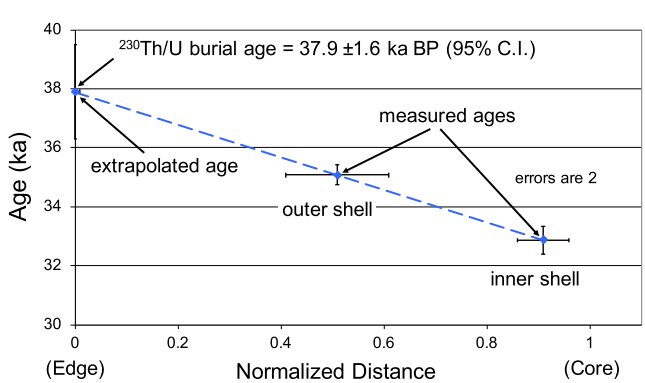


**Fig. 8.** Determining a$^{230}$Th/U burial age from measured $^{230}$Th/U ages of outer and inner shell fractions. Data shown are those for eggshell 140-150-D, which has replicate radiocarbon ages of 39.0–36.1 and 38.7–36.0 ka cal BP (95%) determined at Queen's University Belfast and U. of Arizona, respectively.

## 4. Discussion

Although we expect that $^{230}$Th/U dating of eggshell will be most useful beyond the limit of $^{14}$C dating (ca. 45–50 ka), this study was designed to test our new approach to $^{230}$Th/U dating of ostrich eggshells in a context where the resulting $^{230}$Th/U ages could be compared with reliable and precise independent ages from $^{14}$C dating. The results are encouraging. We observed a relatively high success rate with seven out of nine samples yielding $^{230}$Th/U burial dates. Those ages are in good agreement with $^{14}$C dates on corresponding eggshell carbonate. Uncertainties on the $^{230}$Th/U burial ages have a median value of 5.6% (2σ), facilitating a rigorous assessment of concordance with the $^{14}$C dates. Older eggshells, which tend to have higher ($^{230}$Th/$^{232}$Th) ratios due to greater ingrowth of radiogenic $^{230}$Th, will tend to yield $^{230}$Th/U burial ages with lower relative uncertainties. For example, the median uncertainty of $^{230}$Th/U burial ages >30 ka reported herein is ~4%, making them more precise than many Quaternary chronometers applicable to stratified archaeological contexts. The $^{230}$Th/U burial dating technique also provides reliability criteria inherent to the results for each eggshell, allowing inaccurate $^{230}$Th/U dates to be identified using the $^{230}$Th/U data alone. That is, eggshells with $^{230}$Th/U inner shell ages older than their $^{230}$Th/U outer shell ages have likely lost U, making their $^{230}$Th/U inner shell ages unreliable.

To our knowledge, the spatial distribution of U in ostrich eggshell has not previously been characterized and U uptake in ostrich eggshell has not been studied. Nonetheless, it seems likely that U uptake in ostrich eggshell is qualitatively similar to that in bone, which takes place by some combination of adsorption onto crystal surfaces, lattice substitution (both subject to charge balance), and incorporation into authigenic minerals filling porosity (Trueman and Tuross, 2002). However, we suggest that significant differences between eggshells and bones (and teeth) may influence the duration and complexity of U uptake in each material. That is, compared to bones and teeth – the terrestrial biogenic materials most widely used for $^{230}$Th/U dating – ostrich eggshells are likely to be compositionally and structurally far more stable during burial. During burial, bones lose their large primary organic fraction (ca. 40%, mostly collagen) creating porosity and exposing original nanometer-scale Ca-phosphate crystallites to diagenetic fluids. Fossil bone commonly has low porosity and little residual collagen, indicating that authigenic minerals must replace the lost collagen, a process that likely continues until neomineralization closes down intercrystalline porosity. Studies of archaeological bones indicate that this may take from $10^3$ to $10^5$ years (Person et al., 1996). Bones also commonly acquire U concentrations of tens of ppm or more (e.g., Pike et al., 2002). As a result, U depletion haloes may form around them and reactions involving U source minerals may eventually limit U availability (rather than diffusive transport), perhaps leading to variable U levels at the bone surface over time (see Kohn and Moses, 2013).

Teeth consist of two highly contrasting materials, dentin and enamel. Fine-grained, organic-rich dentin is somewhat similar to bone and can become extremely rich in secondary U (up to 100,000 ppm), causing boundary conditions governing U uptake in adjacent enamel to evolve radically over time, and leading to steep, geometrically complex gradients in U concentrations in enamel as

revealed by laser ablation mapping (e.g., Kohn, 2008; Grun et al., 2008). Such factors likely promote extended and in some cases, multi-stage U mobility in bones and tooth enamel, potentially complicating their use for $^{230}$Th/U and ESR dating (e.g., Pike et al., 2002).

In contrast, eggshells have much lower primary organic content (~3%; Brooks et al., 1990; Miller et al., 2000). Furthermore, some eggshell organics are in intracrystalline sites where they are shielded by surrounding carbonate and remain protected on $10^6$-year timescales (Demarchi et al., 2016; Miller et al., 2016). It follows that far less secondary porosity is created by hydrolization and loss of collagen in eggshells than in bones and dentin. Eggshells are relatively coarse-grained (with crystal sizes of tens to hundreds of μm), and consist of low-Mg calcite (Dalbeck and Cusack, 2006) that is relatively stable under vadose zone conditions in soils of arid to semi-arid regions typical of ostrich habitats. Visible preservation of primary features in eggshell carbonate tens of thousands of years old is consistent with this expectation (e.g., Fig. 3). The much lower U concentrations of archaeological eggshells (median U = 0.03 ppm in this study) relative to bones and teeth are qualitatively consistent with a smaller specific surface area of eggshell carbonate and/or reduced degree of neomineralization inferred from the above considerations. Such low secondary U concentrations likely reduce or eliminate any U depletion halo effects, perhaps simplifying U uptake. Eggshells are also geometrically simple with regard to both external shape and internal layering, facilitating diffusion modeling. We suggest that such differences tend to reduce the duration and complexity of U uptake in eggshell and may contribute to the relatively high success rate of $^{230}$Th/U burial dating observed in this study.

Our study calls attention to two effects of diagenesis on ostrich eggshells with possible consequences for other trace element and isotopic systems in eggshells: 1) relatively pervasive uptake of secondary elements (e.g., U), and 2) the presence of secondary carbonate in macroscopic pores. Our laser ablation analyses confirm that secondary carbonate is present in macroscopic pores of eggshells (see Fig. 5), as inferred by Loewy et al. (2017) who reported more consistent $^{230}$Th/U ages of eggshells after mechanically removing carbonate in pores. Elevated U concentrations spatially associated with such pores have limited extent, however, suggesting the pores did not serve as important conduits for U uptake in the surrounding eggshell. Nonetheless, the presence of secondary carbonate in macroscopic pores, and perhaps also in intercrystalline eggshell porosity, may have consequences not only for $^{230}$Th/U dating but also for $^{14}$C dating and other trace element and isotopic studies of ratite eggshells. For example, it is unclear if conventional acid pretreatment of eggshells for $^{14}$C dating is successful in removing such secondary carbonate. If not, such carbonate could cause $^{14}$C dates on in eggshells to be "too young" (e.g., Miller et al., 1999). Likewise, the primary Sr isotopic composition of eggshell, which may be useful in determining its geographic origin (e.g., Beard and Johnson, 2000), may be subject to modification by isotopically distinct Sr contained in secondary carbonate.

The techniques and results of this study may be pertinent to $^{230}$Th/U dating of eggshells of other ratites given their similar structure and composition (Dalbeck and Cusack, 2006; Mikhailov, 1997; Nys et al., 2004; Szczerbińska and Wiercińska, 2014). Ratites including the ostrich, emu, rhea, the extinct *Genyornis*, and others were common during the late Quaternary in arid to semi-arid environments in Africa, the Near East, the rest of Asia (prior to their Holocene extirpation), South America, Australia and elsewhere. Moreover, C, N, and O isotopes of ratite eggshells can provide paleoenvironmental proxy records of vegetation, precipitation, and other parameters (e.g., Johnson et al., 1997, Johnson et al., 1998; Miller and Fogel, 2016; Newsome et al., 2011; Niespolo et al., 2017b; Niespolo et al., 2018; Von Schirnding et al., 1982). Thus, $^{230}$Th/U dating of ratite eggshell is potentially applicable to Middle Pleistocene to Holocene archaeological and paleoenvironmental studies over a broad geographic range. We suggest that the wide distribution of ratite eggshells, the relatively high success rate of $^{230}$Th/U burial dating observed in this study, and the tractable effort required to produce $^{230}$Th/U burial dates make it attractive to use $^{230}$Th/U dating of eggshells to provide robust time axes for diverse Quaternary terrestrial stratigraphic sequences.

## 5. Conclusions

We have studied U-Th systems in a modern ostrich eggshell and in nine eggshells from a Pleistocene-Holocene archaeological site in east Africa. Petrographic study indicates that ancient eggshells preserve primary structures similar to those of modern eggshell, consisting of layers of low-Mg calcite crystals of varying size and orientation. Proceeding inward, the ~2-mm thick eggshells consist of the vertical crystal layer (~0.1 mm), the palisade layer (~1.4 mm), and the mammillary cone layer (~0.5 mm).

U is very low in the modern eggshell (<1 ppb), with higher levels in the analyzed archaeological eggshells (median = 33 ppb), consistent with secondary uptake of U in archaeological eggshells. Laser ablation profiles and maps of eggshells reveal that secondary U concentrations vary by ca. 100-fold across the ~2-mm thick eggshells. All eggshells studied show U concentration profiles with broadly similar, asymmetric shapes. Changes in U concentration and gradient are spatially correlated with transitions in the layered eggshell structure indicating that U uptake is structurally modulated.

Laser ablation analyses reveal that common Th — i.e., $^{232}$Th, which serves as an index of extraneous $^{230}$Th from detritus —— occurs at high levels adjacent to eggshell surfaces and along macroscopic pores. $^{232}$Th occurs at much lower levels in eggshell interiors, making such carbonate highly suitable for $^{230}$Th/U dating. Guided by the U and $^{232}$Th profiles of each eggshell, selective abrasion can be used to isolate eggshell carbonate with optimal U and Th levels for $^{230}$Th/U dating.

Analyses of eggshell carbonate via solution ICP-MS techniques show that most eggshells (seven out of nine) yield $^{230}$Th/U ages that become younger with increasing distance from the eggshell's outer surface. Such a pattern is consistent with progressive inward transport of secondary U, followed by fixation and decay to $^{230}$Th, yielding $^{230}$Th/U inner shell ages $\leq$ $^{230}$Th/U outer shell ages.

Two of nine eggshells fail to conform to the above pattern — i.e., their $^{230}$Th/U inner shell ages are older than their $^{230}$Th/U outer shell ages. These two eggshells also have $^{230}$Th/U inner shell ages that are older than the $^{14}$C dates of corresponding eggshell carbonate. The anomalously old $^{230}$Th/U ages likely result from loss of U after a period of decay to $^{230}$Th and indicate that in some cases U can be redistributed or lost from eggshells. Determining $^{230}$Th/U ages of at least two fractions of carbonate therefore provides a criterion for assessing the reliability of individual $^{230}$Th/U eggshell ages.

Improved estimates of eggshell age were obtained by using a diffusion model to correct measured $^{230}$Th/U ages for the effect of prolonged U uptake. We term such model ages "$^{230}$Th/U burial ages". Good agreement between $^{230}$Th/U burial ages and $^{14}$C ages of Lukenya Hill eggshells indicates that $^{230}$Th/U burial ages are reliable estimates of eggshell age.

We are conducting ongoing studies to determine if favorable properties of ostrich eggshells for $^{230}$Th/U dating persist in eggshells older than those of this study. If so, then $^{230}$Th/U dating of eggshells will be particularly useful beyond the limit of $^{14}$C dating (ca. 50 ka) and may be useful to the limit of the $^{230}$Th/U system itself

at ca. 500 ka.

## Acknowledgements

This research is based on work supported by the National Science Foundation under grant no.BCS-1727085 to W.D.S. and C.A.T., Harvard University, the American School of Prehistoric Research, and the Ann and Gordon Getty Foundation. We thank Christina Polito Halter for carrying out U-Th separation chemistry and the staff of the National Museums of Kenya. Work in Kenya was conducted under Research Permits NCST/5/002/R/576 issued to C.A.T. and NACOSTI/P/15/4186/6890 to J.T.F. by the Government of the Republic of Kenya while affiliates of the National Museums of Kenya.

## Appendix A. Supplementary data

Supplementary data to this article can be found online at https://doi.org/10.1016/j.quascirev.2019.06.037.

## References

Ambrose, S.H., 1998. Chronology of the later stone age and food production in east Africa. J. Archaeol. Sci. 25, 377–392.
Arsuaga, J.L., Martínez, I., Arnold, L.J., Aranburu, A., Gracia-Téllez, A., Sharp, W.D., Quam, R.M., Falguères, C., et al., 2014. Neandertal roots: cranial and chronological evidence from Sima de los Huesos. Science 344, 1358–1363.
Beard, B.L., Johnson, C.M., 2000. Strontium isotope composition of skeletal material can determine the birth place and geographic mobility of humans and animals. J. Forensic Sci. 45 (5), 1049–1061.
Bird, M.I., Turney, C.S.M., Fifield, L.K., Smith, M.A., Miller, G.H., Roberts, R.G., et al., 2003. Radiocarbon dating of organic- and carbonate-carbon in *Genyornis* and *Dromaius* eggshell using stepped combustion and stepped acidification. Quat. Sci. Rev. 22, 1805–1812.
Blegen, N., Tryon, C.A., Faith, J.T., Peppe, D.J., Beverly, E.J., Li, B., Jacobs, Z., 2015. Distal tephras of the eastern Lake Victoria basin, equatorial East Africa: correlations, chronology, and a context for early modern humans. Quat. Sci. Rev. 122, 89–111. https://doi.org/10.1016/j.quascirev.2015.04.024.
Bronk Ramsey, C., 2008. Radiocarbon dating: revolutions in understanding. Archaeometry 50 (2), 249–275.
Brooks, A.S., Hare, P.E., Kokis, J.E., Miller, G.H., Ernst, R.D., Wendorf, F., 1990. Dating Pleistocene archeological sites by protein diagenesis in ostrich eggshell. Science 248, 60–64.
Cheng, H., Edwards, R.L., Shen, C.-C., Polyak, V.J., Asmerom, Y., Woodhead, J., Hellstrom, J., Wang, Yongjin, Kong, Xinggong, Spotl, C., Wang, Xianfeng, Alexander Jr., E.C., 2013. Improvements in $^{230}$Th dating, $^{230}$Th and $^{234}$U half-life values, and U-Th isotopic measurements by multi-collector inductively coupled plasma mass spectrometry. Earth Planet. Sci. Lett. 371–372, 82–91.
Cheng, H., Edwards, R.L., Southon, J., Matsumoto, K., Feinberg, J.M., Sinha, A., et al., 2018. Atmospheric $^{14}$C/$^{12}$C changes during the last glacial period from Hulu Cave. Science 362, 1293–1297.
Dalbeck, P., Cusack, M., 2006. Crystallography (electron backscatter diffraction) and chemistry (electron probe microanalysis) of the avian eggshell. Cryst. Growth Des. 6 (11), 2558–2562.
Demarchi, B., Hall, S., Roncal-Herrero, T., Freeman, C.L., Wooley, J., Crisp, M.K., et al., 2016. Protein sequences bound to mineral surfaces persist into deep time. eLife 2016 (5), e17092. https://doi.org/10.7554/eLife.17092.
Edwards, R.L., Gallup, C.D., Cheng, H., 2003. Uranium-series dating of marine and lacustrine carbonates. In: Bourdon, B., Henderson, G.M., Lundstrom, C.C., Turner, S.P. (Eds.), Uranium-Series Geochemistry, Reviews in Mineralogy & Geochemistry, vol. 52. Mineralogical Society of America, Washington, DC, U.S.A., pp. 363–405
Elliott, J.C., 2002. Calcium phosphate biominerals. Rev. Mineral. Geochem. 48 (1), 427–453.
Galbraith, R.F., Roberts, R.G., 2012. Statistical aspects of equivalent dose and error calculation and display in OSL dating: an overview and some recommendations. Quat. Geochronol. 11, 1–27.
Galbraith, R.F., Roberts, R.G., Laslett, G.M., Yoshida, H., Olley, J.M., 1999. Optical dating of single and multiple grains of quartz from Jinmium rock shelter, northern Australia: Part I, experimental design and statistical models. Archaeometry 41, 339–364.
Gliganic, L.A., Jacobs, Z., Roberts, R.G., Dominguez-Rodrigo, M., Mabulla, A.Z., 2012. New ages for Middle and Later Stone Age deposits at Mumba rockshelter, Tanzania: optically stimulated luminescence dating of quartz and feldspar grains. J. Hum. Evol. 62 (4), 533–547.
Gramly, R.M., 1976. Upper Pleistocene archaeological occurrences at site GvJm/22, Lukenya Hill, Kenya. Man 11, 319–344. https://doi.org/10.2307/2800274.
Grün, R., 2007. Electron spin resonance dating. In: Encyclopedia of Quaternary Science. Elsevier, Oxford, pp. 1505–1516.
Grün, R., Aubert, M., Joannes-Boyau, R., Moncel, M.-H., 2008. High resolution analysis of uranium and thorium concentration as well as U-series isotope distributions in a Neanderthal tooth from Payre (Ardeche, France) using laser ablation ICP-MS. Geochem. Cosmochim. Acta 72, 5278–5290.
Grün, R., Eggins, S., Kinsley, L., Moseley, H., Sambridge, M., 2014. Laser ablation U-series analyses of fossil bones and teeth. Palaeogeogr. Palaeoclimatol. Palaeoecol. 416, 150–167.
Hellstrom, J., Pickering, R., 2015. Recent advances and future prospects of the U-Th and U-Pb chronometers applicable to archaeology. J. Archaeol. Sci. 56, 32–40.
Hoffmann, D.L., Standish, C.D., García-Diez, M., Pettitt, P.B., Milton, J.A., Zilhão, J., Alcolea-González, J.J., Cantalejo-Duarte, P., Collado, H., de Balbín, R., Lorblanchet, M., Ramos-Muñoz, J., Weniger, G.-Ch., Pike, A.W.G., 2018. U-Th dating of carbonate crusts reveals Neandertal origin of Iberian cave art. Science 359, 912–915.
Holden, N.E., 1989. Total and spontaneous fission half-lives for uranium, plutonium, americium and curium nuclides. Pure Appl. Chem. 61, 1483–1504.
Holen, S.R., Deméré, T.A., Fisher, D.C., Fullagar, R., Paces, J.B., Jefferson, G.T., et al., 2017. A 130,000-year-old archaeological site in southern California, USA. Nature 544 (7651), 479–485. https://doi.org/10.1038/nature22065.
Jacobs, Z., Roberts, R.G., Galbraith, R.F., Deacon, H.J., Grün, R., Mackay, A., Mitchell, P., Vogelsang, R., Wadley, L., 2008. Ages for the Middle Stone Age of southern Africa: implications for human behavior and dispersal. Science 322, 733–735.
Jacobs, Z., Hayes, E.H., Roberts, R.G., Galbraith, R.F., Henshilwood, C.S., 2013. An improved OSL chronology for the Still Bay layers at Blombos Cave, South Africa: further tests of single-grain dating procedures and a re-evaluation of the timing of the Still Bay industry across southern Africa. J. Archaeol. Sci. 40, 579–594.
Jaffey, A.H., Flynn, K.F., Glendenin, L.E., Bentley, W.C., Essling, A.M., 1971. Precise measurement of half-lives and specific activities of $^{235}$U and $^{238}$U. Phys. Rev. C 4, 1889–1906.
Jain, S., Bajpai, S., Kumar, G., Pruthi, V., 2016. Microstructure, crystallography and diagenetic alteration in fossil ostrich eggshells from Upper Palaeolithic sites of Indian peninsular region. Micron 84, 72–78.
Janz, L., Elston, R.G., Burr, G.S., 2009. Dating North Asian surface assemblages with ostrich eggshell: implications for palaeoecology and extirpation. J. Archaeol. Sci. 36, 1982–1989.
Johnson, B.J., Miller, G.H., Fogel, M.L., Beaumont, P.B., 1997. The determination of late Quaternary paleoenvironments at Equus Cave, South Africa, using stable isotopes and amino acid racemization in ostrich eggshell. Palaeogeogr. Palaeoclimatol. Palaeoecol. 136, 121–137.
Johnson, B.J., Fogel, M.L., Miller, G.H., 1998. Stable isotopes in modern ostrich eggshell: a calibration for paleoenvironmental applications in semi-arid regions of Southern Africa. Geochem. Cosmochim. Acta 62, 2451–2461.
Kohn, M.J., 2008. Models of diffusion-limited uptake of trace elements in fossils and rates of fossilization. Geochem. Cosmochim. Acta 72, 3758-2770.
Kohn, M.J., Moses, R.J., 2013. Trace element diffusivities in bone rule out simple diffusive uptake during fossilization but explain in vivo uptake and release. Proc. Natl. Acad. Sci. Unit. States Am. 110, 419–424. https://doi.org/10.1073/pnas.1209513110.
Lane, C.S., Chorn, B.T., Johnson, T.C., 2013. Ash from the Toba supereruption in Lake Malawi shows no volcanic winter in East Africa at 75 ka. Proc. Natl. Acad. Sci. Unit. States Am. 110 (20), 8025–8029.
Lane, C.S., Brauer, A., Martin-Puertas, C., Blockley, S.P.E., Smith, V.C., Tomlinson, E.L., 2015. The Late Quaternary tephrostratigraphy of annually laminated sediments from Meerfelder Maar, Germany. Quat. Sci. Rev. 122, 192–206.
Loewy, S.L., Valdes, J., Yanny, S.J.W., De La Cruz, K., Banner, J.L., Kappelman, J., Todd, L., 2017. More accurate U - Th ages of ostrich eggshells (OES) with improved sample processing. Geol. Soc. Am. Abstr. Progr. 49 (6) https://doi.org/10.1130/abs/2017AM-308572. ISSN 0016-7592.
Ludwig, K.R., 2010. Using Isoplot/Ex, Version 3.75: A Geochronological Toolkit for Microsoft Excel. Berkeley Geochronology Center Special Publication 1a, Berkeley, California, p. 47. Berkeley Geochronology Center.
Ludwig, K.R., Paces, J.B., 2002. Uranium-series dating of pedogenic silica and carbonate, Crater Flat, Nevada. Geochim. Comochim. Acta 66, 487–506.
Ludwig, K.R., Wallace, A.R., Simmons, K.R., 1985. The Schwartzwalder uranium deposit, II: age of uranium mineralization and Pb-isotope constraints on genesis. Econ. Geol. 80, 1858–1871.
Magee, J.W., Bowler, J.M., Williams, D.L.G., 1995. Stratigraphy, sedimentology, chronology and paleohydrology of quaternary lacustrine deposits at Madigan Gulf, lake Eyre, South Australia. Palaeogeogr. Palaeoclimatol. Palaeoecol. 113, 3–42.
Magee, J.W., Miller, G.H., Spooner, N.A., Questiaux, D.G., McCulloch, M.T., Clark, P.A., 2009. Evaluating Quaternary dating methods: radiocarbon, U-series, luminescence, and amino acid racemization dates of a later Pleistocene emu egg. Quat. Geochronol. 4, 84–92.
Marean, C.W., Bar-Matthews, M., Bernatchez, J., Fisher, E., Goldberg, P., Herries, A.I.R., Jacobs, Z., Jerardino, A., Karkanas, P., Minichillo, T., Nilssen, P.J., Thompson, E., Watts, I., Williams, H.M., 2007. Early Human use of marine resources and pigment in South Africa during the Middle Pleistocene. Nature 449, 905–908. https://doi.org/10.1038/nature06204.
Matheron, G., 1973. The intrinsic random functions and their applications. Adv. Appl. Probab. 5, 439–468.
McBrearty, S., Brooks, A.S., 2000. The revolution that wasn't: a new interpretation of the origin of modern human behavior. J. Hum. Evol. 39, 453–563.
McGuire, A., 2015. The Potential of Cryptotephra as a Geochronological Tool at

Lukenya Hill Cave and Panga Ya Saidi Rockshelter, East Africa. M.Sc. thesis. The University of Manchester.
Mertz-Kraus, R., Jochum, K.P., Sharp, W.D., Stoll, B., Weis, U., Andreae, M.O., 2010. In situ Th-230-Th-232-U-234-U-238 analysis of silicate glasses and carbonates using laser ablation single-collector sector-field ICP-MS. J. Anal. At. Spectrom. 25 (12), 1895–1904.
Mikhailov, K., 1997. Fossil and recent eggshell in amniotic vertebrates: fine structure, comparative morphology and classification. Spec. Pap. Palaeontol. 56, 1–76.
Millard, A.R., Hedges, R.E.M., 1996. A diffusion-absorption model of uranium uptake by archaeological bone. Geochim. Comochim. Acta 60, 2139–2152.
Miller, G.H., Fogel, M.L., 2016. Calibrating δ18O in Dromaius novaehollandiae (emu) eggshell calcite as a paleo-aridity proxy for the Quaternary of Australia. Geochem. Cosmochim. Acta 193, 1–13. https://doi.org/10.1016/j.gca.2016.08.004.
Miller, G.H., Magee, J.W., Johnson, B.J., Fogel, M.L., Spooner, N.A., McCulloch, M.T., Ayliffe, L.K., 1999. Pleistocene extinction of Genyornis newtoni: human impact on Australian megafauna. Science 283, 205–208.
Miller, G.H., Hart, C.P., Roark, E.B., Johnson, B.J., 2000. Isoleucine epimerization in eggshells of the flightless Australian birds, Genyornis and Dromaius. In: Goodfriend, G.A., Collins, M.J., Fogel, M.L., Macko, S.A., Wehmiller, J.F. (Eds.), Perspectives in Amino Acid and Protein Geochemistry. Oxford Univesity Press., N.Y.
Miller, G.H., Fogel, M.L., Magee, J.W., Gagan, M.K., 2016. Disentangling the impacts of climate and human colonization on the flora and fauna of the Australian arid zone over the past 100 ka using stable isotopes in avian eggshell. Quat. Sci. Rev. 151, 27–57.
Newsome, S.D., Miller, G.H., Magee, J.W., Fogel, M.L., 2011. Quaternary record of aridity and mean annual precipitation based on δ15N in ratite and dromornithid eggshells from Lake Eyre, Australia. Oecologia 167, 1151–1162. https://doi.org/10.1007/s00442-011-2046-5.
Niespolo, E.M., Sharp, W.D., Fylstra, N., Tryon, C.A., Weisz, D.G., Faith, J.T., Henshilwood, C.S., Lewis, J., Mackay, A., Steele, T., Van Niekerk, K., 2017a. Patterns of Secondary U in Ostrich Eggshell: Application to U-Th Dating of Quaternary Terrestrial Strata. Goldschmidt Abstracts, p. 2914.
Niespolo, E.M., Sharp, W.D., Tryon, C.A., Faith, J.T., Lewis, J., Dawson, T.E., 2017b. C and N stable isotopes in Late Pleistocene-Holocene ostrich eggshells reveal distinct local paleoenvironments in East Africa during the MSA-LSA transition. In: Paleoanthropology Society Annual Meeting.
Niespolo, E.M., Sharp, W.D., Tryon, C.A., Faith, J.T., Lewis, J., Ranhorn, K.L., Mambelli, S., Miller, M.J., Dawson, T.E., 2018. Site-specific Paleoenvironmental Records during the Middle-To-Later Stone Age Transition at Kisese II and Lukenya Hill Using Light Stable Isotopes of Ostrich Eggshells. Geological Society of America Fall Meeting, Poster.
Nys, Y., Gautron, J., Garcia-Ruiz, J.M., Hinke, M.T., 2004. Avian eggshell mineralization: biochemical and functional characterization of matrix proteins. Gen. Palaeontol. (Palaeobiochem.) 3, 549–562.
Oerter, E.J., Sharp, W.D., Oster, J.L., Ebeling, A., Valley, J.W., Kozdon, R., Orland, I.J., Hellstrom, J., Woodhead, J.D., Hergt, J.M., Chadwick, O.A., Amundson, R., 2016. Anomalous North American atmospheric circulation 70,000 to 55,000 years ago. Proc. Natl. Acad. Sci. Unit. States Am. 113, 919–924. https://doi.org/10.1073/pnas.1515478113.
Person, A., Bocherens, H., Mariotti, A., Reynard, M., 1996. Diagenetic evolution and experimental heating of bone phosphate. Palaeogeogr. Palaeoclim. Palaeoecol. 126, 135–150.
Pickering, R., Herries, A.I.R., Woodhead, J.D., Hellstrom, J.C., Green, H.E., Paul, B., Ritzman, T., Strait, D.S., Schoville, B.J., Hancox, P.J., 2019. U–Pb-dated flowstones restrict South African early hominin record to dry climate phases. Nature 565, 226–229. https://doi.org/10.1038/s41586-018-0711-0.
Pike, A.W.G., Hedges, R.E.M., Van Calsteren, P., 2002. U-series dating of bone using the diffusion-adsorption model. Geochim. Comochim. Acta 66, 4273–4286.
Ranhorn, K., Tryon, C.A., 2018. New radiocarbon dates from Nasera rockshelter (Tanzania): implications for studying spatial patterns in late Pleistocene Technology. J. Afr. Archaeol. 16, 1–12.
Richter, D., Grün, R., Joannes-Boyau, R., Steele, T.E., Amani, F., Rué, M., Fernandes, P., Raynal, J.P., Geraads, D., Ben-Ncer, A., Hublin, J.-J., McPherron, S.P., 2017. The age of the hominin fossils from Jebel Irhoud, Morocco, and the origins of the middle stone age. Nature 296, 293–296.
Rink, W.J., Richter, D., Schwarcz, H.P., Marks, A.E., Monigal, K., Kaufman, D., 2003. Age of the middle palaeolithic site of Rosh Ein mor, central Negev, Israel: implications for the age range of the early Levantine mousterian of the Levantine corridor. J. Archaeol. Sci. 30, 195–204.
Roberts, R.G., Jones, R., Smith, M.A., 1994. Beyond the radiocarbon barrier in Australian prehistory. Antiquity 68, 611–616.
Roberts, R.G., Jacobs, Z., Li, B., Jankowski, N.R., Cunningham, A.C., Rosenfeld, A.B., 2015. Optical dating in archaeology: thirty years in retrospect and grand challenges for the future. J. Archaeol. Sci. 56, 41–60.
Sambridge, M., Grün, R., Eggins, S., 2012. U-series dating of bone in an open system: the diffusion-adsorption-decay model. Quat. Geochronol. 9, 42–53.
Schwarcz, H.P., Morawska, L., 1993. Uranium-series dating of carbonates from Bir tarfawi and Bir Sahara east. In: Wendorf, F., Schild, R., Close, A.E. (Eds.), Egypt during the Last Interglacial: the Middle Paleolithic of Bir Tarfawi and Bir Sahara East. Springer Science+Business media, New York, pp. 205–217.
Sharp, W.D., Paces, J.B., 2018. Comment on "The earliest modern humans outside Africa". Science 362, eaat6598. https://doi.org/10.1126/science.aat6598.
Sharp, W.D., Ludwig, K.R., Chadwick, O.A., Amundson, R., Glaser, L.L., 2003. Dating fluvial terraces by $^{230}$Th/U on pedogenic carbonate, wind river basin, Wyoming. Quat. Res. 59, 139–150.
Sharp, W.D., Mertz-Kraus, R., Valverdu, J., Bischoff, J.L., Vaquero, M., 2016. Archeological deposits at Abric Romaní extend to 110 ka: U-series dating of a newly cored, 30 meter-thick section. J. Archaeol. Sci. Rep. 5, 400–406.
Skonieczny, C., McGee, D., Winkler, G., Bory, A., Bradtmiller, L.I., Kinsley, C.W., et al., 2019. Monsoon-driven Saharan dust variability over the past 240,000 years. Sci. Adv. 5 (1), eaav1887.
Smith, E.I., Jacobs, Z., Johnsen, R., Ren, M., Fisher, E., Oestmo, S., Wilkins, J., Harris, J.A., Karkanas, P., Fitch, S., Ciravolo, A., Keenan, D., Cleghorn, N., Lane, C.S., Matthews, T., Marean, C.W., 2018. Humans thrived in South Africa through the Toba eruption about 74,000 years ago. Nature 555, 511–515.
Szczerbińska, D., Wiercińska, M., 2014. Ultrastructure of the eggshell of selected palaeognathae species – a comparative analysis. Ann. Anim. Sci. 14, 167–178. https://doi.org/10.2478/aoas-2013-0079.
Texier, P.J., Porraz, G., Parkington, J., Rigaud, J.P., Poggenpoel, C., Miller, C., Tribolo, C., Cartwright, C., Coudenneau, A., Klein, R., Steele, T., Verna, C., 2010. A Howiesons Poort tradition of engraving ostrich eggshell containers dated to 60,000 years ago at Diepkloof Rock Shelter, South Africa. Proc. Natl. Acad. Sci. U. S. A 107, 6180–6185. https://doi.org/10.1073/pnas.0913047107.
Trueman, C.N., Tuross, N., 2002. Trace elements in recent and fossil bone apatite. Rev. Mineral. Geochem. 48 (1), 489–521.
Tryon, C.A., Crevecoeur, I., Faith, J.T., Ekshtain, R., Nivens, J., Patterson, D., Mbua, E.N., Spoor, F., 2015. Late Pleistocene age and archaeological context for the hominin calvaria from GvJm-22 (Lukenya Hill, Kenya). Proc. Natl. Acad. Sci. U.S.A. 112 (9), 2682–2687.
Tryon, C.A., Lewis, J.E., Ranhorn, K.L., Kwekason, A., Alex, B., Laird, M.F., Marean, C.W., Niespolo, E., Nivens, J., Audax, Z.P., Mabulla, A.Z.P., 2018. Middle and later stone age chronology of Kisese II rockshelter (UNESCO World Heritage Kondoa rock-art sites), Tanzania. PLoS One 13 (2), e0192029. https://doi.org/10.1371/journal.pone.0192029.
Vogel, J.C., Visser, E., Fuls, A., 2001. Suitability of ostrich eggshell for radiocarbon dating. Radiocarbon 43, 133–137.
Von Schirnding, Y., Van der Merwe, N.J., Vogel, J.C., 1982. Influence of diet and age on carbon isotope ratios in ostrich eggshell. Archaeometry 24, 3–20.
Wang, C.-X., Zhang, Y., Gao, X., Wang, H.-M., 2009. Archaeological study of ostrich eggshell beads collected from SDG site. Chin. Sci. Bull. 54, 3887–3895. https://doi.org/10.1007/s11434-009-0620-6.